NRL Memorandum Report 4034

AD A075 063

The Non-Linear Theory of Free Electron Lasers and Efficiency Enhancement

P. SPRANGLE

Plasma Physics Division

CHA-MEI TANG

Icpor, Alexandria, VA

W. M. MANHEIMER

Plasma Physics Division

LEVEL II

September 28, 1979

NAVAL RESEARCH LABORATORY
Washington, D.C.

SECURITY CLASSIFICATION OF THIS PAGE (When Data Entered)

REPORT DOCUMENTATION PAGE

READ INSTRUCTIONS BEFORE COMPLETING FORM

1. REPORT NUMBER: NRL Memorandum Report 4034
2. GOVT ACCESSION NO.
3. RECIPIENT'S CATALOG NUMBER
4. TITLE (and Subtitle): THE NON-LINEAR THEORY OF FREE ELECTRON LASERS AND EFFICIENCY ENHANCEMENT.
5. TYPE OF REPORT & PERIOD COVERED: Interim report on a continuing NRL problem.
6. PERFORMING ORG. REPORT NUMBER
7. AUTHOR(s): P. Sprangle, Cha-Mei Tang, W. M. Manheimer
8. CONTRACT OR GRANT NUMBER(s): DARPA Contract No. 3817
9. PERFORMING ORGANIZATION NAME AND ADDRESS: Naval Research Laboratory, Washington, D.C. 20375
10. PROGRAM ELEMENT, PROJECT, TASK AREA & WORK UNIT NUMBERS: NRL Problem 67R18-16B and 67R08-59; ONR Project No. RR011-09-41
11. CONTROLLING OFFICE NAME AND ADDRESS
12. REPORT DATE: September 28, 1979
13. NUMBER OF PAGES: 52
14. MONITORING AGENCY NAME & ADDRESS (if different from Controlling Office)
15. SECURITY CLASS. (of this report): Unclassified
15a. DECLASSIFICATION/DOWNGRADING SCHEDULE
16. DISTRIBUTION STATEMENT (of this Report): Approved for public release; distribution unlimited
17. DISTRIBUTION STATEMENT (of the abstract entered in Block 20, if different from Report)
18. SUPPLEMENTARY NOTES: *Jaycor, Alexandria, Va.
19. KEY WORDS (Continue on reverse side if necessary and identify by block number): Free electron lasers; Efficiency enhancement; Non-linear theory
20. ABSTRACT (Continue on reverse side if necessary and identify by block number)

The development of lasers in which the active medium is a relativistic stream of free electrons has recently evoked much interest. The potential advantages of such free electron lasers include, among other things, continuous frequency tunability, very high power of operations and high efficiency. The free electron laser is characterized by a pump field; for example, a spatially periodic magnetic field, which scatters from a relativistic electron beam. The scattered radiation has a wavelength much smaller than the pump wavelength depending on the electron

(Continued)

DD FORM 1 JAN 73 1473 EDITION OF 1 NOV 65 IS OBSOLETE
S/N 0102-014-6601

SECURITY CLASSIFICATION OF THIS PAGE (When Data Entered)

393 453

20. ABSTRACT (Continued)

beam energy. We present a general self-consistent non-linear theory of the free electron laser process. The non-linear formulation of the temporal steady state free electron laser problem results in a set of coupled differential equations governing the spatial evolution of the amplitudes and wavelength of the radiation and space charge fields. These equations are readily solved numerically since the amplitude and wavelength vary on a spatial scale which is comparable to a growth length of the output radiation. A number of numerical/analytical illustrations are presented ranging from the optical to the submillimeter wavelength regime. Our non-linear formulation in the linear regime is compared with linear theory and agreement is found to be excellent. Analytical expressions for the saturated efficiency and radiation amplitude are also shown to be in very good agreement with our non-linear numerical solutions. Efficiency curves are obtained for both the optical and submillimeter FEL examples with fixed magnetic pump parameters. We show that these intrinsic efficiencies can be greatly enhanced by appropriately contouring the magnetic pump period. In the case of the optical FEL, the theoretical single pass efficiency can be greater than 20% by appropriately decreasing the pump period and increasing the pump magnetic field.

CONTENTS

I. INTRODUCTION 1

II. NON-LINEAR EVOLUTION OF SCATTERED WAVES 4

III. DERIVATION OF NON-LINEAR DRIVING CURRENTS 7

IV. PARTICLE ORBIT EQUATIONS 11

V. DERIVATION OF LINEAR GROWTH RATES, EFFICIENCIES AND SATURATION FIELD AMPLITUDES 15

VI. RESULTS AND DISCUSSION 18

ACKNOWLEDGMENTS 24

APPENDIX A — General Non-Linear Formulation 25

REFERENCES 29

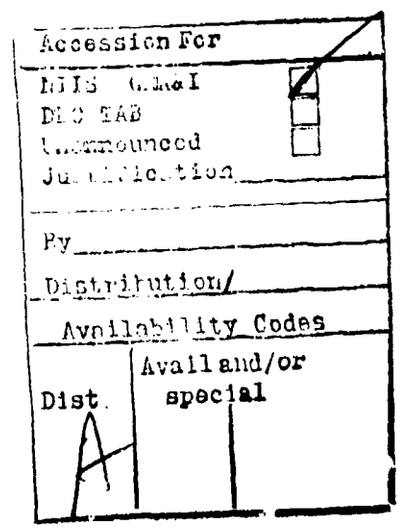

THE NON-LINEAR THEORY OF FREE ELECTRON LASERS AND EFFICIENCY ENHANCEMENT

1. INTRODUCTION

Free electron lasers (FELs) based on backscattering from relativistic electron beams have demonstrated a unique potential for becoming a new type of coherent radiation source. In principle, these radiation sources will be characterized by output wavelengths ranging from the millimeter to beyond the optical regime, frequency tunability, very high power levels and high efficiencies.

Theoretical analysis on the FEL mechanism has been carried out in the single particle[1-18] as well as the collective scattering regime.[7,11,15,17-26] Also, non-linear processes and saturation efficiencies have been considered for various FEL scattering regimes.[6,8,15,17,18,23,24,27]

The operative mechanism in FELs is a parametric process in which a long wavelength pump field interacts with a beam of relativistic electrons. Under certain conditions the incident pump field will decay into a longitudinal wave (density wave) and a backscattered electromagnetic wave which is double doppler upshifted in frequency. The longitudinal wave (also referred to as density wave, beat wave or ponderomotive wave) results from the coupling of the pump field and the electromagnetic field through the $\mathbf{v} \times \mathbf{B}/c$ force term. The ponderomotive wave plays a central role in the linear and non-linear development of the scattering process. Its

Manuscript submitted July 19, 1979.

effects on the electron beam is closely analogous to the role played by the negative energy (slow space charge) wave in conventional traveling wave mechanisms.

The pump field may take the form of a static spatially periodic magnetic or electric field or a propagating electromagnetic wave. In this paper we take the pump to be a static, periodic right-handed, helically polarized, magnetic field. The frequency of the scattered radiation is given by

$$\omega \approx (1 + v_z/c)\ \gamma_z^2\, v_z(2\pi/l) \approx 4\pi\gamma_z^2 c/l,$$

where

$$\gamma_z = (1 - v_z^2/c^2)^{-1/2},$$

v_z is the axial beam velocity and l is the pump period. The possibility of using a two-stage FEL scattering process, in order to reduce the electron energy required for very short output wavelengths, has been suggested.[14,18]

Roughly speaking, FELs can be divided into two categories, depending on the gain of the radiation field. In the low gain regime, the overall spatially integrated gain is due to wave interference effects and is much less than unity. This is a single particle (collective effects are not manifested through space charge fields) scattering regime and is exemplified by experiments at Stanford University.[28,29]

The high gain FELs are characterized by stimulated radiation fields which grow exponentially in the linear regime. Experiments with intense relativistic electron beams performed at NRL, Columbia University and Cornell University fall into this class.[30–35] For a detailed theoretical discussion of the various FEL mechanisms the reader is referred to Refs. (11), (17) and (18).

The main objectives of this work are to present a self-consistent non-linear formulation of the FEL mechanism and to theoretically analyze some of the concepts necessary to develop efficient, high power, tunable FEL radiation sources. Some of the salient features of this theory include: i) completely arbitrary magnetic pump field (period and amplitude can be functions of axial position) ii) space charge effects, iii) arbitrary polarization of the radiation field, iv) completely relativistic particle dynamics and v) frequency and spatial harmonics in the excited fields. The non-linear formalism developed for the FEL problem is also applicable to a large class of temporal steady state convective processes. Our formulation of the problem permits the spatial dependence of the pump magnetic field to be arbitrary. Hence, efficiency enhancement schemes which utilize amplitude and wavelength spatial variations of the pump field can be analyzed. The spatial variation of the scattered radiation amplitude and wavelength occurs on a scale-length which is large compared to the wavelength of the pump field. This permits numerical solutions for cases where the electron beam energy is extremely high. That is, in this approach, there is no large separation of spatial scale lengths, despite the large spatial scale difference between the wavelength of the scattered field and the pump field, so arbitrarily high values of the relativistic gamma factor, γ, associated with the beam, can be considered. Furthermore, the formulation is carried out in the laboratory frame under temporal steady state conditions.

The analytical formulation of the general non-linear steady state FEL problem consists essentially of three parts. In section II, the wave equations are used to derive expressions for the slow spatial evolution of the amplitudes and phases of the scattered fields in terms of the driving currents. Then, in section III, the driving currents are expressed as functions of the dynamics of the particle ensemble (electron distribution function). The particle orbit equations are written self-consistently in terms of the scattered fields in section IV. The orbit equations describing the motion transverse and parallel to the electron stream are completely decoupled.

The linear spatial growth rates, efficiencies and saturated field amplitudes are derived in section V for various scattering regimes. Finally a number of analytical/numerical illustrations in the high gain scattering regime are given in section VI. The non-linear particle dynamics is discussed in some detail. Efficiency curves are obtained, and a method of dramatically increasing the single pass efficiency, as suggested in Ref. (17), by contouring both the pump period and magnetic field is analyzed.[36] For instance, efficiency of >20% are shown to be theoretically possible at optical wavelengths using this approach. The basic idea is to gradually slow down the phase velocity of the ponderomotive wave at the point where the electrons are deeply trapped in the ponderomotive wave potentials. The slowing down of the wave is accomplished by adiabatically decreasing the pump field period. Appendix A contains the formulation of the FEL process with spatial and temporal harmonics in both the radiation and space charge fields. Also included in this formulation is the ability of the radiation field to undergo a change in polarization from a circularly polarized to an elliptically polarized wave as the particle dynamics become non-linear.

The resulting set of non-linear coupled equations self-consistently relate the spatial dynamics of the particles and fields. These equations have been solved analytically in the linear approximation and the linear dispersion relation was obtained. The full set of non-linear coupled equations are readily solved numerically for the spatial growth rate and saturation level of the scattered fields.

II. NON-LINEAR EVOLUTION OF SCATTERED WAVES

The physical model which we will develop is that of a fully relativistic electron beam interacting with a spatially periodic pump magnetic field as depicted in Fig. (1). Only spatial variations along the z axis will be considered for the electron beam, pump field and scattered radiation field.

The variable amplitude and period pump magnetic field can be expressed in terms of the vector potential

$$\mathbf{A}_0(z) = A_0(z)\left\{\cos\left[\int_0^z k_0(z')dz'\right]\hat{e}_x + \sin\left[\int_0^z k_0(z')dz'\right]\hat{e}_y\right\}, \tag{1}$$

where the amplitude $A_0(z)$ and wavenumber $k_0(z)$ are known and slowly varying functions of z. The potential field in (1) is a good approximation to a right-handed polarized helical magnetic field near the z-axis of an appropriate coil winding. The pump magnetic field associated with (1) is given by

$$\mathbf{B}_0(z) = B_0(z)\left\{\cos\left[\int_0^z k_0(z')dz' + \varphi(z)\right]\hat{e}_x + \sin\left[\int_0^z k_0(z')dz' + \varphi(z)\right]\hat{e}_y\right\}, \tag{2}$$

where

$$B_0(z) = -\left((k_0(z)A_0(z))^2 + (\partial A_0(z)/\partial z)^2\right)^{1/2}$$

and

$$\varphi(z) = -\tan^{-1}\left[\frac{\partial A_0(z)/\partial z}{k_0(z)A_0(z)}\right]$$

are slowly varying functions of z. The period of the magnetic field is

$$l(z) = 2\pi/(k_0(z) + \partial\varphi/\partial z) \approx 2\pi/k_0(z). \tag{3}$$

The scattered electromagnetic and electrostatic fields in terms of the vector potential $\mathbf{A}(z,t)$ and scalar potential $\phi(z,t)$ are taken to be

$$\mathbf{A}(z,t) = A_x(z)\cos\left[\int_0^z k_+(z')dz' - \omega t + \theta\right]\hat{e}_x - A_y(z)\sin\left[\int_0^z k_+(z')dz' - \omega t + \theta)\right]\hat{e}_y,$$

$$\phi(z,t) = \phi(z)\cos\left[\int_0^z k(z')dz' - \omega t + \theta_z\right], \tag{4a,b}$$

where the amplitudes of the potentials, $A_x(z)$, $A_y(z)$ and $\phi(z)$ as well as the wavenumbers $k_+(z)$ and $k(z)$ are slowly varying functions of z. The scattered electromagnetic field represented by Eq. (4a) is a right-handed elliptically polarized field traveling towards the right.

The frequency ω of the field and the phases, θ and θ_z, are independent of z. In appendix A, the general form for the scattered fields is used in the non-linear formulation of the problem. However, in the main body of the text, the fields in Eqs. (4) will be used in order to minimize the notational algebra.

The evolution of the scattered potentials is governed by the wave equations

$$\left(\frac{\partial^2}{\partial z^2} - \frac{1}{c^2}\frac{\partial^2}{\partial t^2}\right) \mathbf{A}(z,t) = -\frac{4\pi}{c}\mathbf{J}_\perp(z,t),$$

and

$$\frac{\partial^2 \psi(z,t)}{\partial z \partial t} = 4\pi J_z(z,t), \tag{5a,b}$$

where $\mathbf{J}(z,t)$ is the driving current density. Substituting the potentials of Eqs. (4) into (5) we obtain

$$(\omega^2/c^2 - k_+^2(z))\, A_x(z)\cos\psi(z,t)$$

$$-2k_+^{1/2}(z)\frac{\partial}{\partial z}\left(A_x(z)k_+^{1/2}(z)\right)\sin\psi(z,t) = -\frac{4\pi}{c}J_x(z,t),$$

$$(\omega^2/c^2 - k_+^2(z))\, A_y(z)\sin\psi(z,t)$$

$$+2k_+^{1/2}\frac{\partial}{\partial z}\left(A_y(z)\,k_+^{1/2}(z)\right)\cos\psi(z,t) = \frac{4\pi}{c}J_y(z,t),$$

$$\frac{\partial\phi(z)}{\partial z}\sin\psi_z(z,t) + k(z)\,\phi(z)\cos\psi_z(z,t) = \frac{4\pi}{\omega}J_z(z,t), \tag{6a,b,c}$$

where

$$\psi(z,t) = \int_0^z k_+(z')\,dz' - \omega t + \theta,$$

and

$$\psi_z(z,t) = \int_0^z k(z')\,dz' - \omega t + \theta_z.$$

Terms proportional to $\partial^2 A/\partial z^2$ have been neglected from (6). The neglect of $\partial^2 A/\partial z^2$ terms is not central to our formulation, though it can be shown to be an excellent approximation which

simplifies the final FEL equations. The coefficients of the sinusoidal terms on the left hand side of Eqs. (6) are slowly varying functions of z and independent of t. The arguments of the sinusoidal terms on the other hand are rapidly varying function of t for z fixed. The rapidly time varying terms, in for example Eq. (6a), can be removed by multiplying it by $\begin{matrix}\cos\\ \sin\end{matrix}\psi(z,t)$ and taking the temporal average over one wave period, i.e., $(\omega/2\pi)\int_0^{2\pi/\omega} dt$. Performing this operation on Eq. (6a) as well as similar ones on Eqs. (6b,c) we obtain

$$(\omega^2/c^2 - k_+^2(z))\, A_x(z) = \frac{-4\omega}{c}\int_0^{2\pi/\omega} J_x(z,t)\cos\psi(z,t)\, dt,$$

$$2k_+^{1/2}(z)\frac{\partial}{\partial z}\left(A_x(z)k_+^{1/2}(z)\right) = \frac{4\omega}{c}\int_0^{2\pi/\omega} J_x(z,t)\sin\psi(z,t)\, dt,$$

$$(\omega^2/c^2 - k_+^2(z))\, A_y(z) = \frac{4\omega}{c}\int_0^{2\pi/\omega} J_y(z,t)\sin\psi(z,t)\, dt,$$

$$2k_+^{1/2}(z)\frac{\partial}{\partial z}\left(A_y(z)k_+^{1/2}(z)\right) = \frac{4\omega}{c}\int_0^{2\pi/\omega} J_y(z,t)\cos\psi(z,t)\, dt,$$

$$\frac{\partial\phi(z)}{\partial z} = 4\int_0^{2\pi/\omega} J_z(z,t)\sin\psi_z(z,t)\, dt,$$

$$k(z)\,\phi(z) = 4\int_0^{2\pi/\omega} J_z(z,t)\cos\psi_z(z,t)\, dt. \qquad (7a\text{-}f)$$

III. DERIVATION OF NON-LINEAR DRIVING CURRENTS

It is now necessary to derive expressions for the x, y and z components of the current densities and perform the time integration specified in Eqs. (7). In general the non-thermal electron distribution function, written in terms of the electron orbits, is

$$f(z,\mathbf{p},t) = n_0 v_{z0}\int_{-\infty}^{\infty}\delta(z-\xi(t_0,t))\,\delta(p_x-\eta_x(t_0,t))\,\delta(p_y-\eta_y(t_0,t))\,\delta(p_z-\eta_z(t_0,t))\,dt_0 \qquad (8)$$

where n_0 is the uniform particle density to the left of the interaction region, i.e., $z \leqslant 0$, v_{z0} is the constant axial electron velocity for $z \leqslant 0$, $\xi(t_0,t)$ is the axial position of the particle at

time t which crossed the $z = 0$ plane at time t_0 and $\underline{\eta}(t_0, t)$ is the momentum vector of the particle at time t which crossed the $z = 0$ plane at time t_0. Thermal effects which are characteristic of actual electron beams can be easily included by appropriately modifying the electron distribution function in (8). The integral over t_0 in Eq. (8) takes into account the continuous flow of particles into the interaction region. The current density associated with this electron distribution is

$$\mathbf{J}(z, t) = -|e| \int \frac{\mathbf{p}}{\gamma(\mathbf{p}) m_0} f(z, \mathbf{p}, t) d^3\mathbf{p}$$
$$= \frac{-|e| n_0 v_{z0}}{m_0} \int_{-\infty}^{\infty} \frac{\underline{\eta}(t_0, t)}{\gamma(\underline{\eta}(t_0, t))} \delta(z - \xi(t_0, t)) dt_0, \tag{9}$$

where $\gamma(\underline{\eta}) = (1 + \underline{\eta}^2/m_0^2 c^2)^{1/2}$. As will be seen later it is necessary to rewrite Eq. (9) in the form

$$\mathbf{J}(z, t) = \frac{-|e| n_0 v_{z0}}{m_0} \int_{-\infty}^{\infty} \frac{\underline{\eta}(t_0, t) \delta(t - \tau(t_0, z))}{\gamma(\underline{\eta}(t_0, t)) |\partial \xi(t_0, t)/\partial t|} dt_0, \tag{10}$$

where

$$\tau(t_0, z) = t_0 + \int_0^z \frac{dz'}{v_z(t_0, z')} \tag{11}$$

is the time it takes a particle to reach the position z if it entered the interaction region, $z = 0$, at time t_0 and $v_z(t_0, z)$ is the axial velocity of a particle at position z which was at $z = 0$ at time t_0.

The quantity $\partial \xi(t_0, t)/\partial t$ is the axial velocity v_z of a particle at time t which was at $z = 0$ at time t_0. Clearly, for $\mathbf{J}(z, t)$ to be finite, v_z should not vanish in the interaction region. If v_z vanishes and particles are turned around, multi-streaming develops and the entire concept of $\exp(-i\omega t)$ being the only time dependence is undermined (due to, for instance, two-stream instabilities). We assume here that no particle is slowed down to zero velocity in the laboratory frame, hence

$$\gamma(\underline{\eta}(t_0, t)) m_0 |\partial \xi(t_0, t)/\partial t| = \eta_z(t_0, t). \tag{12}$$

Substituting (12) into (10), the general form for the driving current becomes

$$\mathbf{J}(z, t) = -|e| n_0 v_{z0} \int_{-\infty}^{\infty} \frac{\eta(t_0, t)}{\eta_z(t_0, t)} \delta(t - \tau(t_0, z)) dt_0. \tag{13}$$

Substituting the above form for $\mathbf{J}(z, t)$ into the right-hand-side of Eqs. (7), we obtain the self-consistent amplitudes and phases of the scattered potentials in terms of driving currents. To show how the right-hand-sides of Eqs. (7) can be reduced by using Eq. (13), we simplify Eq. (7a) as an illustration.

Substituting the x-component of Eq. (13) into (7a) gives

$$(\omega^2/c^2 - k_+^2(z)) A_x(z) = \int_0^{2\pi/\omega} dt \int_{-\infty}^{\infty} dt_0 \, G_x(t_0, z, t) \, \delta(t - \tau(t_0, z)), \tag{14a}$$

where

$$G_x(t_0, z, t) = 4\frac{\omega}{c} |e| n_0 v_{z0} \frac{\eta_x(t_0, t)}{\eta_z(t_0, t)} \cos \psi(z,t). \tag{14b}$$

Since the system of particles and fields are in the temporal steady state, particles which cross the $z = 0$ plane separated in time by $2\pi/\omega$ will execute identical orbits which are separated in time by $2\pi/\omega$. It is, therefore, possible to define an initial beam segment, "beamlet," for which all possible steady state orbits of the actual beam particles are represented by the particles in the beamlet, but are displaced in time. The axial length of the beamlet is clearly $2\pi v_{z0}/\omega$. With these considerations in mind we find that the function $G_x(t_0,z,t)$ and $\tau(t_0, z)$ have certain periodic properties in their arguments which permit the integrals in (14) to be greatly simplified. Specifically we note that

$$G_x(t_0, z,t) = G_x\left(t_0 + \frac{2\pi N}{\omega}, z, t + \frac{2\pi N}{\omega}\right),$$

and

$$\tau(t_0, z) = \tau\left(t_0 + \frac{2\pi N}{\omega}, z\right) - \frac{2\pi N}{\omega}, \tag{15a,b}$$

where $N = 0, \pm 1, \pm 2, \ldots$. The t integration in Eq. (14a) is over one wave period, 0 to $2\pi/\omega$. From Eq. (15b) we see that over this range of t the argument of the delta function will vanish over an interval in t_0 equal to $2\pi/\omega$. Therefore, it is not necessary to integrate over t_0 from $-\infty$ to $+\infty$. Finally from the property of $G_x(t_0, z,t)$ expressed in (15a) we find that

$$\int_0^{2\pi/\omega} dt \int_{-\infty}^{\infty} dt_o\, G_x(t_o, z, t)\, \delta(t - \tau(t_o, z))$$

$$= \int_0^{2\pi/\omega} G_x(t_o, z, \tau(t_o, z))\, dt_o. \tag{16}$$

This can be seen most easily in a diagram, of the region of integration in Fig. 2, where the entire (t, t_o) plane is broken into squares of $2\pi/\omega$ on a side. Because of the symmetry property expressed in Eqs. (15a) and (15b), the value of the integrand is unchanged along a diagonal; this is indicated by certain squares having the same letter. Clearly then, an integral in the vertical direction, over the shaded squares, is the same as an integral in the horizontal direction, over the slashed squares. Substituting (16) together with (14b) into (14a) results in a simplified form for Eq. (7a). All the integrals on the right hand side of Eqs. (7) can be reduced in exactly the same way. Doing this we find that Eqs. (7) can be put into the form

$$(\omega^2/c^2 - k_+^2(z))\, A_x(z) = 4\,|e|\, n_o \frac{v_{z0}}{c}\, \omega \int_0^{2\pi/\omega} \frac{\eta_x(t_o, \tau(t_o, z))}{\eta_z(t_o, \tau(t_o, z))} \cos\psi(z, \tau(t_o, z))\, dt_o,$$

$$2k_+^{1/2}(z)\, \frac{\partial}{\partial z}(A_x(z)\, k_+^{1/2}(z)) = -4\,|e|\, n_o \frac{v_{z0}}{c}\, \omega \int_0^{2\pi/\omega} \frac{\eta_x(t_o, \tau(t_o, z))}{\eta_z(t_o, \tau(t_o, z))} \sin\psi(z, \tau(t_o, z))\, dt_o,$$

$$(\omega^2/c^2 - k_+^2(z))\, A_y(z) = -4\,|e|\, n_o \frac{v_{z0}}{c}\, \omega \int_0^{2\pi/\omega} \frac{\eta_y(t_o, \tau(t_o, z))}{\eta_z(t_o, \tau(t_o, z))} \sin\psi(z, \tau(t_o, z))\, dt_o,$$

$$2k_+^{1/2}(z)\, \frac{\partial}{\partial z}\,(A_y(z)\, k_+^{1/2}(z)) = -4\,|e|\, n_o \frac{v_{z0}}{c}\, \omega \int_0^{2\pi/\omega} \frac{\eta_y(t_o, \tau(t_o, z))}{\eta_z(t_o, \tau(t_o, z))} \cos\psi(z, \tau(t_o, z))\, dt_o,$$

$$\frac{\partial\phi(z)}{\partial z} = -4\,|e|\, n_o\, v_{z0} \int_0^{2\pi/\omega} \sin\psi_z(z, \tau(t_o, z))\, dt_o,$$

$$k(z)\,\phi(z) = -4\,|e|\, n_o\, v_{z0} \int_0^{2\pi/\omega} \cos\psi_z(z, \tau(t_o, z))\, dt_o. \tag{17a-f}$$

Notice that on the right-hand-side of the above equations the single integrals over t_o are from 0 to $2\pi/\omega$. As we will see, these integrals can be evaluated numerically by following the orbits of a relatively small number of particles which enter the interaction region in any single time interval of duration $2\pi/\omega$. Upon deriving the general orbit equations for the particle ensemble, in the next section, we will assume that the scattered electromagnetic wave is circularly polarized, i.e., $A_x(z) = A_y(z)$. This assumption is clearly not central to our formulation.

IV. PARTICLE ORBIT EQUATIONS

We now express the particle orbits, which are needed for the evaluation of Eqs. (17) in terms of the new independent variables t_o and z. The forces exerted on the electrons arise from the pump and scattered potentials given in Eqs. (1) and (4). We immediately note that the transverse canonical momenta of the particles is conserved. Therefore, if both the pump and scattered fields are zero as $z \to -\infty$, the transverse particle momenta are given by

$$p_x(z,\ t) = \frac{|e|}{c}\,(A_{ox}(z) + A_x(z,\ t)),$$

and

$$p_y(z,\ t) = \frac{|e|}{c}(A_{oy}(z) + A_y(z,\ t)). \tag{18a,b}$$

Using Eqs. (18) the longitudinal component of the force equation can be put into the form

$$\frac{dp_z(z,\ t)}{dt} = \frac{-|e|^2}{2\gamma(z,\ t)\ m_o c^2}\left[\frac{\partial}{\partial z}(\mathbf{A}_o(z) + \mathbf{A}(z,\ t))^2 - 2\gamma(z,\ t)\ \frac{m_o c^2}{|e|}\ \frac{\partial}{\partial z}\ \phi(z,\ t)\right], \tag{19}$$

where $p_z(z,\ t)$ is the axial momentum and the relativistic gamma factor is

$$\gamma(z,\ t) = \left[1 + \frac{|e|^2}{m_o^2 c^4}\ (\mathbf{A}_o(z) + \mathbf{A}(z,\ t))^2 + \frac{p_z^2(z,\ t)}{m_o^2 c^2}\right]^{1/2}. \tag{20}$$

Equations (18), (19) and (20) specify the particle dynamics in terms of the pump and scattered fields. The transverse and longitudinal particle motion is formally decoupled. To write Eqs. (18) and (19) in terms of the new independent variables z and t_o, we note that

$$t = \tau(t_o, z) = t_o + \int_0^z dz'/v_z(t_o, z'),$$

$$\frac{d}{dt} = V_z(z, \tau)\,\frac{d}{dz},$$

where $V_z(z, \tau) = v_z(t_o, z)$. Note that $\frac{d}{dz}$ (which follows a particle orbit) $\neq \frac{\partial}{\partial z}$ (which is taken at constant time).

In terms of z and τ we simply get

$$p_x(z, \tau) = \frac{|e|}{c}\,(A_{ox}(z) + A_x(z, \tau)),$$

$$p_y(z, \tau) = \frac{|e|}{c}\,(A_{oy}(z) + A_y(z, \tau)),$$

$$\frac{dp_z^2(z, \tau)}{dz} = -\frac{|e|^2}{c^2}\left[\frac{\partial}{\partial z}(\mathbf{A}_o(z) + \mathbf{A}(z, \tau))^2 - 2\gamma(z, \tau)\,\frac{m_o c^2}{|e|}\,\frac{\partial}{\partial z}\,\phi(z, \tau)\right]. \quad (21a,b,c)$$

We have expressed the particle orbits in terms of the entry time t_o and axial position z. Note that our definition of the momenta implies that, $\eta_x(t_o, \tau) = p_x(z, \tau)$, $\eta_y(t_o, \tau) = p_y(z, \tau)$, and $\eta_z(t_o, \tau) = p_z(z, \tau) = \gamma(z, \tau)\, m_o V_z(z, \tau)$. At this point we take the scattered electromagnetic wave to be circularly polarized and set $A_x(z) = A_y(z) = A(z)$. To obtain the final set of equations for the amplitude $A(z)$ and wavenumber $k_+(z)$ we first combine Eqs. (17a) and (17b) with Eqs. (17c) and (17d) respectively. Using the expressions for η_x and η_y given by Eqs. (21a,b) we arrive at the following expressions

$$(\omega^2/c^2 - k_+^2(z))\,A(z) = \frac{\omega_b^2}{2c^2}\, m_o v_{zo}\,\frac{\omega}{\pi}\int_0^{2\pi/\omega} \eta_z^{-1}(t_o, \tau(t_o, z))$$

$$\left\{A_o(z)\cos\left[\int_0^z (k_+(z') + k_o(z'))\,dz' - \omega\,\tau(t_o, z) + \theta\right] + A(z)\right\} dt_o.$$

$$2k_+^{1/2}(z)\,\frac{\partial}{\partial z}(A(z)\,k_+^{1/2}(z)) = -\frac{\omega_b^2}{2c^2}\,m_o v_{zo}\,\frac{\omega}{\pi}\int_0^{2\pi/\omega}\eta_z^{-1}(t_o,\,\tau(t_o,\,z))$$

$$\left\{A_o(z)\,\sin\left[\int_0^z (k_+(z') + k_o(z'))\,dz' - \omega\tau(t_o,\,z) + \theta\right]\right\}dt_o. \qquad (22a,b)$$

where we have used Eqs. (1) and (4a) for $\mathbf{A}_o(z)$ and $\mathbf{A}(z,\,t)$ and $\omega_b = (4\pi|e|^2\,n_o/m_o)^{1/2}$.

For completeness we rewrite Eqs. (17e) and (17f) for the scalar potential

$$\frac{\delta\phi(z)}{\delta z} = \frac{-\omega_b^2}{c^2}\,\frac{v_{zo}}{\pi}\,\frac{m_o c^2}{|e|}\int_o^{2\pi/\omega}\sin\left[\int_o^z k(z')dz' - \omega\tau(t_o,z) + \theta_z\right]dt_o,$$

$$k(z)\,\phi(z) = \frac{-\omega_b^2}{c^2}\,\frac{v_{zo}}{\pi}\,\frac{m_o c^2}{|e|}\int_o^{2\pi/\omega}\cos\left[\int_o^z k(z')dz' - \omega\tau(t_o,z) + \theta_z\right]dt_o. \qquad (23a,b)$$

The relevant particle dynamics is contained in Eq. (21b) which is rewritten in the form

$$\frac{d\eta_z^2(t_o,\tau)}{dz} = \frac{-|e|^2}{c^2}\left[\frac{\partial}{\partial z}\,(\mathbf{A}_o(z) + \mathbf{A}(z,\tau))^2 - 2\gamma(z,\tau)\frac{m_o c^2}{|e|}\,\frac{\partial\phi(z,\tau)}{\partial z}\right] \qquad (24)$$

where

$$\gamma(z,\tau) = \left[1 + \frac{|e|^2}{m_o^2 c^4}|\mathbf{A}_o(z) + \mathbf{A}\,(z,\tau)|^2 + \frac{\eta_z^2(t_o,\tau)}{m_o^2 c^2}\right]^{1/2},$$

$$\tau(t_o,z) = t_o + \int_o^z \frac{\gamma(z',\tau(t_o,z'))\,m_o}{\eta_z(t_o,\tau(t_o,z'))}dz',$$

$$(\mathbf{A}_o(z) + \mathbf{A}(z,\tau))^2 = A_o^2(z) + A^2(z)$$

$$+ 2A_o(z)A(z)\cos\left[\int_o^z (k_+(z') + k_o(z'))dz' - \omega\tau + \theta\right]. \qquad (25a,b,c)$$

The non-linear formulation of the FEL is fully described by Eqs. (22), (23) and (24). The ponderomotive potential plays a central role in axially bunching the electron. From Eq. (24) we see that this potential is given by

$$\phi_{pond}(z,\tau) = \frac{-|e|}{\gamma_o m_o c^2}\,A_o(z)A(z)\cos\left[\int_0^z (k_+(z') + k_o(z'))\,dz' - \omega\tau + \theta\right]. \qquad (26)$$

The amplitude and phase of the scattered fields as well as the axial beam momentum all vary with a characteristic axial length which is much longer than the pump wavelength l. This fact allows for inexpensive numerical simulations to be performed in the laboratory frame with extremely high gamma electron beams.

To see that the system quantities vary on a scale length long compared to l, we note that the characteristic length, as estimated from the arguments of the sinusoidal terms on the right-hand-side of Eqs. (22), (23) and (24), is roughly equal to $L \approx (k_+ + k_o - \omega/v_z)^{-1}$. However, since the frequency of the scattered radiation is $\omega = ck \approx (1 + \beta_z)\, \gamma_z^2 v_z\, k_o$, we find that

$$L >> 1/k_o = l/2\pi.$$

This fact permits us to solve numerically the FEL equations for arbitrarily high gamma beams. The more conventional simulation approaches suffer from the problem of large temporal or spatial scale differences even in the beam frame of reference.

To complete our formulation of FELs we need an expression for the efficiency. The efficiency can be defined as the ratio of the electromagnetic energy flux increase to the initial electron energy flux, that is

$$\eta = \frac{c}{4\pi} \frac{<\mathbf{E}(z,t) \times \mathbf{B}(z,t)>_t - <\mathbf{E}(o,t) \times \mathbf{B}(o,t)>_t}{v_{zo} n_o (\gamma_o - 1) m_o c^2}, \tag{27}$$

where $\mathbf{E} = c^{-1}\partial \mathbf{A}/\partial t$, $\mathbf{B} = \hat{e}_z \times \partial \mathbf{A}/\partial z$, $<\cdots>_t$ denotes an average over the field period $2\pi/\omega$, and v_{zo} n_o and γ_o are the initial beam axial velocity, density and total gamma factor.

Using the vector potential in Eq. (4a) and taking the radiation field to the circularly polarized, i.e., $A_x = A_y = A$, the efficiency in Eq. (27) takes the form

$$\eta = \left(\frac{|e|}{m_o c}\right)^2 \frac{\omega}{\omega_b^2} \frac{(k_+(z) A^2(z) - k_+(0) A^2(0))}{v_{zo}\, (\gamma_o - 1)} \tag{28}$$

and is maximum when the radiation fields saturate.

V. DERIVATION OF LINEAR GROWTH RATES, EFFICIENCIES AND SATURATION FIELD AMPLITUDES

In this section we present the salient features of the FEL in the linear regime. Results for the linear growth rate and expressions for the saturation efficiency and radiation amplitude are obtained in the high gain case, i.e., where the radiation field amplitude has e-folded at least a few times. For a more detailed derivation of these quantities see Refs. (17) and (18).

In the high gain linear regime the excited space charge and vector potentials are of the form

$$\phi(z,t) = \frac{\tilde{\phi}(0)}{2} e^{i(kz-\omega t)} + c.c.,$$

$$\mathbf{A}(z,t) = \frac{\tilde{A}(0)}{2} e^{i(k_+ z-\omega t)}(\hat{e}_x + i\hat{e}_y) + c.c., \tag{29}$$

where $\tilde{\phi}(0)$ and $\tilde{A}(0)$ are the potential amplitudes at the input end of the interaction region, $z=0$, and the wavenumbers, k and k_+ are complex and independent of z. For a magnetic pump of the form in Eq.(1) with constant amplitude and period and cold electron beam, the dispersion relation is

$$D(\omega,\ k_+)\ ((\omega - v_{zo}k)^2 - \omega_b^2/(\gamma_{zo}^2\gamma_o)) = -\frac{\omega_b^2}{2\gamma_o}\ (\beta_{zo}\ \beta_{o\perp})^2\ D(\omega,\ k), \tag{30}$$

where $D(\omega,\ k) = \omega^2 - c^2k^2 - \omega_b^2/\gamma_o$, $k_+ = k - k_o$, k_o is the pump wavenumber, $\omega_b = (4\pi|e|^2 n_o/m_o)^{1/2}$ is the beam plasma frequency, v_{zo} is the axial beam velocity, $v_{o\perp} = |e|B_o/(\gamma_o m_o c k_o)$ is the transverse beam velocity, B_o is the pump amplitude, $\gamma_o = (1 - \beta_{zo}^2 - \beta_{o\perp}^2)^{-1/2}$, $\beta_{o\perp} = v_{o\perp}/c$, $\beta_{zo} = v_{zo}/c$ and $\gamma_{zo} = (1 - \beta_{zo})^{-1/2}$. Since the electromagnetic wave approximately satisfies the dispersion relation $\omega/c \approx k_+$ we can replace $D(\omega,\ k_+)$ and $D(\omega,\ k)$ by $-2k_+(k_+ - (\omega^2 - \omega_b^2/\gamma_o)^{1/2}/c)$ and $-2k\ k_o c^2$ respectively. The dispersion relation can now be put into the simple form

$$\delta k\ (\delta k + 2\xi\ k_o/\gamma_{zo})(\delta k - \Delta k) = -\alpha^2 k_o/2, \tag{31}$$

where $k = \omega/v_{zo} + \xi\, k_o/\gamma_{zo} + \delta k$, δk is complex, $|\delta k| << k$, $\xi = \omega_b/(\sqrt{\gamma_o}\, c\, k_o)$, $\Delta k = k_o - \omega/(2c\gamma_{zo}^2)$, and $\alpha^2 = (\xi\beta_{o\perp}\, k_o)^2$. Equation (31) assumes that the beam is relativistic $v_{zo} \approx c$ and $\omega >> \omega_b/\sqrt{\gamma_o}$. Two distinct regimes can be distinguished from the dispersion relation in (31).

a) Weak Magnetic Pump Limit

For a pump magnetic field strength such that $\beta_{o\perp} << \beta_{crit} \equiv 4(\xi/\gamma_{zo}^3)^{1/2}$ the space charge potential dominates the ponderomotive potential and collective effects play an important role. In this regime of scattering the dispersion relation in (31) yields

$$\delta k = \frac{\Delta k}{2} - \frac{i}{2}\sqrt{\alpha^2\,\gamma_{zo}/\xi - (\Delta k)^2} \tag{32}$$

for the growing root. Maximum spatial linear growth occurs when there is no frequency mismatch, i.e., $\Delta k = 0$ and is given by

$$\Gamma_{max} = -\, Im\ (\delta k)_{max} = \frac{1}{2}\,(\alpha^2\gamma_{zo}/\xi)^{1/2}. \tag{33}$$

b) Strong Magnetic Pump Limit

In this regime, defined by the condition $\beta_{o\perp} >> \beta_{crit}$, space charge forces are dominated by ponderomotive forces. This is a single partice scattering regime and Eq. (31) reduces to

$$(\delta k)^2(\delta k - \Delta k) = -\,\alpha^2\, k_o/2. \tag{34}$$

The maximum spatial linear growth rate according to (34) occurs for exact frequency matching, i.e., $\Delta k = 0$ and is given by

$$\Gamma_{max} = -\, Im\ (\delta k)_{max} = \frac{\sqrt{3}}{2^{4/3}}\,(\xi\beta_{o\perp})^{2/3}k_o. \tag{35}$$

To obtain estimates for the saturation levels in the high gain regimes we resort to heuristic arguments based on electron trapping dynamics. It can be argued that at saturation, when electrons are deeply trapped, the axial velocity of the electron beam has decreased by the

amount $2\Delta v$ where $\Delta v = v_{zo} - v_{ph}$ is the difference between the equilibrium axial beam velocity and the initial phase velocity of the total longitudinal wave, i.e., $v_{ph} = \omega/Re(k)$. The decrease in the particle kinetic energy is

$$\Delta E_{K.E.} \approx 2\gamma_o\gamma_{zo}^2 m_o v_{zo}\Delta v, \tag{36}$$

so the energy conversion efficiency becomes

$$\eta = \frac{\Delta E_{K.E.}}{(\gamma_o - 1)m_o c^2} \approx 2\gamma_{zo}^2 \Delta v/c$$

$$= 2\gamma_{zo}^2(v_{zo} - \omega/Re(k))/c. \tag{37}$$

Substituting $Re(k) = \omega/v_{zo} + \xi k_o/\gamma_{zo} + Re(\delta k)$ and $\omega \approx 2\gamma_{zo}^2 ck_o$ into (37), the expression for efficiency becomes

$$\eta = \xi/\gamma_{zo} + Re(\delta k)/k_c, \tag{38}$$

where $Re(\delta k)$ is determined from the solution of the dispersion relation in (31). Using Eqs. (31) and (38) we find that in the weak pump and strong pump limit the growth rate maximizes when $\Delta k = 0$, i.e., $\omega = 2\gamma_{zo}^2 ck_o$, and the efficiency at saturation is respectively

$$\eta = \xi/\gamma_{zo}, \tag{39}$$

and

$$\eta = 2^{-4/3}(\xi\beta_{o\perp})^{2/3} + \xi/\gamma_{zo}. \tag{40}$$

Applying the conservation law for total energy flux we find that the magnitude of the vector potential at saturation is

$$|A_{sat}| = \left(\frac{\xi\gamma_o}{2\gamma_{zo}^2}\,\frac{m_o c^2}{|e|}\right)\eta^{1/2}. \tag{41}$$

where η is given by either (39) or (40) depending on whether the weak or strong pump limit is applicable.

VI. RESULTS AND DISCUSSION

In this section we present the numerical results for the coupled non-linear FEL equations in (22), (23) and (24). Illustrations for a wide range of parameters ranging from the submillimeter to the optical radiation regime are given. The mono-energetic electron beam enters the interaction region at $z = 0$ with a uniform density. The magnetic pump field given in (1) is assumed to be built up adiabatically from $z \leq 0$ to its initial value at $z = 0$. In all of our numerical simulations a small amplitude radiation field is introduced as a perturbation at $z = 0$ and allowed to grow spatially and self-consistently according to the FEL equations. The small initial radiation field, typically less than 0.1% of the saturated field amplitude, allows for a long spatial region of linear interaction and, hence, for an accurate comparison with the linear theory presented in section V. Furthermore, space charge fields are included in all of our numerical illustrations even though in some cases the ponderomotive field may dominate the process as is the case in the strong magnetic pump scattering limit.

We will first consider two examples where the magnetic pump parameters are fixed, i.e., constant amplitude and period. Furthermore, we will show that efficiency can be increased to a few 10's of percent even in the optical regime by contouring the magnetic pump period and amplitude.

a) Constant Magnetic Pump Illustrations

Two examples will be discussed in some detail: 1) optical radiation at $\lambda = 0.75\ \mu$m from a 66 MeV electron beam and 2) submillimeter radiation at $\lambda = 338\ \mu$m with a 2.6 MeV electron beam. Table I lists the salient parameters for the magnetic pump, electron beam and output radiation of both examples.

For the optical radiation case, example 1, the magnetic pump amplitude is 6.0 kG and the period is fixed at 1.5 cm. The 66 MeV ($\gamma_o = 131$), 2 kA electron beam has a transverse equilibrium velocity of $v_{oi} = 5.4 \times 10^{-3}$ c with the given value of magnetic pump field. The critical transverse velocity, see section V, is $v_{crit} = 1.5 \times 10^{-3}$ c, hence the scattering process is in the strong pump regime.

Figure (3) shows the amplitude of the vector potential of the scattered radiation, $A(z)$, and the spatial growth rate, $\Gamma = \partial(\ln A(z))/\partial z$, as a function of z. Those plots are for an optical frequency of $\omega = 2\gamma_{zo}^2\, ck_o = 2.525 \times 10^{15}$ sec^{-1}. Notice that in Fig. (3) there is a long spatial region where the growth rate is fairly constant. This is the linear region of the interaction. The value of the radiation frequency in this figure has been chosen to maximize the linear growth rate, i.e., zero frequency mismatch, $\Delta k = 0$. The linear e-folding length associated with this output frequency is 38 cm.

Figure (4) shows a comparison between the spatial growth rates obtained from the linear regime of the numerical simulation of our FEL equations (crosses (x)) and the linear growth rates obtained from the dispersion relation in Eq. (30), (solid curve) over the frequency spectrum. These two independent calculations of the linear growth rate are in excellent agreement. Figure (4) also compares the efficiency at saturation obtained by solving the FEL equations (circles (O)) with the calculated values of efficiency using electron trapping arguments (dotted curve) given in section V. Using the value of efficiency for maximum linear growth rate, we find from Eq. (41) that the saturated vector potential amplitude is $A_{sat} = 28$ volts, corresponding to an efficiency of 0.37%, whereas Fig. (3) gives a value of 33 volts for A_{sat}, corresponding to an efficiency of 0.52%. The higher calculated efficiency can be explained by the slight increase of the wave number of the scattered radiation, k_+, just before saturation, solid curve in Fig. (5). When k_+ increases, the phase velocity of the ponderomotive potential,

$\omega/(k_+(z) + k_0(z))$, decreases. As the electrons become trapped at the bottom of the potential well, the ponderomotive wave slows down slightly, hence, the particles are able to transfer more kinetic energy to the scattered radiation. This is clearly a non-linear effect, which linear theory could not predict. The dotted curve in Fig. (5) is the variation of the wave number of the space charge wave. The effects of the space charge wave is negligible, since in the strong pump limit, example 1, the ponderomotive potential is much larger than the space charge potential as can be seen in Fig. (6).

To understand the phenomenon of trapping, phase space plots are a revealing tool. Figures (7a-d), are plots of the relative time the particles in one beamlet cross the following axial positions: $z = 0.0$ m, 2.0 m, 4.0 m, 4.3 m and 4.5 m. Twenty particles are labeled within the beamlet. At the initial position, $z = 0$, the particles enter at equal intervals in time since they have uniform axial velocity, v_{zo}. At $z = 2$ m down stream into the interaction region, the particles are in the linear regime where the growth rate of the scattered radiation is constant. Some particles have gained energy while others have lost energy depending on their phase relation with the ponderomotive potential. At $z = 4$ m, Fig. (7b), the phase space plot begins to show the signs of trapping. Many of the particles are crossing the $z = 4$ m plane at about the same time. However, their velocity spread is large. Figure (7c), at $z = 4.3$ m, depicts the particles before saturation and shows definite signs of trapping. At $z = 4.5$ m, particles labelled 4-9 in Fig. (7d) shows spatial bunching and small velocity spread; these particles are deeply trapped. If the amplitude and period of the magnetic pump field is held fixed, the scattered radiation will reach its maximum value at this axial position.

Our non-linear formulation is also applied to a case where the output radiation is in the submillimeter regime, example 2 in Table I. The pump wavelength and pump magnetic field amplitude are 2 cm and 2.5 kG, respectively. The electron beam energy is 2.6 MeV, ($\gamma_o = 6$);

the beam current is 5 kA and the beam radius is 0.3 cm. The transverse equilibrium velocity is $v_{o\perp} = 0.078$ c, and the critical transverse velocity is $v_{crit} = 0.22$ c. In the example we are barely in the weak-pump regime, since, β_{crit} is less than three times that of $\beta_{o\perp}$. Space charge effects are, therefore, important in this example. Figure (8) is a plot of the space charge and ponderomotive potential for $\omega = 5.05 \times 10^{12}$ sec^{-1} ($\lambda = 338$ μm). This figure shows that collective effects are of the same order of magnitude as the ponderomotive forces.

Figure (9) shows the amplitude of the vector potential amplitude of the scattered radiation, $A(z)$, and the spatial growth rate, $\Gamma = \partial(\ln A(z))/\partial z$, as a function of z for $\omega = 5.05 \times 10^{12}$ sec^{-1}.

Comparing the linear spatial growth rate obtained from the dispersion equation in (30), (solid curve in Fig. (10)), with the growth rate from the linear regime of the non-linear calculation (cross (x)), we again obtain excellent agreement. The theoretical efficiency based on Eqs. (38) and (31) (dotted curve in Fig. (10)) as compared with the results using the non-linear formulation, (circles (O)), is remarkably good. The changes in wave number of the scattered radiation, $k_+(z)$ near saturation (solid curve in Fig. (11)) did not enhance the efficiency because the effect is balanced by the increase in the space charge potential wave.

The particle phase space plots of Figs. (12a-c), are very similar in nature to those in Figs. (7a-d). Figure (12a) contains phase plots at $z = 0.0$ m and 0.35 m corresponding to the initial position and a point in the linear interaction regime. At the $z = 0.7$ m plane just before saturation, Fig. (12b), shows the beginning of particle trapping. Figure (12c) contains the phase space plot when the radiation field has saturated, $z = 0.77$ m.

Figure (13) shows the scaling of the linear spatial growth rate and maximum efficiency as a function of the pump magnetic field amplitude, B_0, at a fixed output frequency. The output

radiation frequency is held constant by requiring that γ_{z0} and k_0 be kept fixed. The electron beam and magnetic pump parameters are basically the same as those of example 1 in Table I, except that the magnetic pump amplitude ranges from 0.25 kG to 6 kG. To keep the frequency fixed, while B_0 is varied, the electron beam energy is changed such that γ_{z0} is held at the constant value of 100. The output frequency used for Fig. (13) is chosen at the maximum growth rate, which is very close to $\omega = 2\gamma_{z0}^2 c\, k_0 = 2.525 \times 10^{15}$ sec^{-1} corresponding to a wavelength of $\lambda = 0.75$ μm. The critical transverse velocity, as discussed in section V, occurs for these parameters at a pump magnetic field of $B_0 = 1.15$ kG. Above this value of pump field the FEL process is in the strong pump regime, while sufficiently below $B_0 = 1.15$ kG the scattering process is in the weak pump regime. In Fig. (13) the crosses (x) denote the linear spatial growth rate obtained from the non-linear simulations, while the solid curve is obtained from the dispersion relation in Eq. (30). Also in this figure is a comparison of efficiency estimated from Eq. (38) using trapping arguments (dashed curve) and actual numerical simulation results (circles (O)).

b) Efficiency Enhancement by Contouring Magnetic Pump Period

According to Eqs. (24) and (26) the phase velocity of the total longitudinal wave potential, i.e. ponderomotive plus space charge is

$$v_{ph} = \omega/(k_+ + k_o) \tag{42}$$

where ω and k_+ are the radiation frequency and wave number and $k_o = 2\pi/l$ is the wave number of the pump field. It has been assumed in writing (42) that the wavenumber of the ponderomotive and space charge waves are identical. The longitudinal wave potential is responsible for axially bunching and eventually trapping the electrons. If the magnetic pump period is held fixed, the radiation field reaches its maximum value when the electrons are trapped at the bottom of the longitudinal potential wells, as can be seen for example in Fig. (7d). Just before

the radiation field saturates, the electrons are somewhat spatially bunched and trapped near the bottom of the wave potential, see Fig. (7c). The trapped electrons at this point can be considered, for our purpose, to form a macro-particle. By appropriately reducing the phase velocity in Eq. (42) as a function of axial distance down the interaction region, the kinetic energy of this macro-particle can be further reduced and converted into wave energy. The phase velocity must be reduced in such a way so that the inertial potential of the trapped macro-particle is always less than the potential of the growing longitudinal wave. According to Eq. (42), the phase velocity can be reduced by decreasing the period of the magnetic pump as a function of z. In order for the macro-particle to remain trapped, the spatial rate of change of the pump period must be sufficiently slow. In principle virtually all the kinetic energy of the macro particle can be extracted and converted to wave energy. However, not all the beam particles comprise the macro-particle; some are untrapped. Converting particle kinetic energy into radiation by varying the wave velocity is somewhat analogous to the reverse process of particle acceleration in say an RF linac. In a wave accelerator, the energy associated with the accelerating slow electromagnetic wave is converted into particle kinetic energy. However, the wave energy in these accelerators does not decay, since it is continuously resupplied by external microwave sources.

We will illustrate efficiency enhancement by contouring the pump period while holding the amplitude of the pump magnetic vector potential constant, using the parameters of example 1 in Table I. The same principle of efficiency enhancement can also be applied to example 2. Figure (7c) shows that a $z = 4.3$ m, the electrons are somewhat spatially bunched at the optical wavelength $\lambda = 0.75\mu$m and the radiation field is nearly saturated. At this point, we simply increased the pump wavenumber $k_o(z)$ exponentially as a function of z instead of optimally contouring the pump period in units of cm^{-1} according to the empirical formula.

$$k_o(z) = \begin{cases} \dfrac{2\pi}{1.5} & z \leqslant z_k \\ \dfrac{2\pi}{1.5} + [\exp(0.002(z-z_k))-1] & z \geqslant z_k \end{cases}$$

where $z_k = 4.3$ m. The period of the magnetic pump, $l(z)$, is depicted in Fig. (14). The spatial decrease of l results in a large increase in the amplitude of the wave vector potential as shown in Fig. (14). For this particular case, the contouring is terminated at $z = 13$ m and the efficiency at this point is already 20%. In principle, the pump wavelength contouring can be continued and even higher efficiencies achieved. Figures (15a-d) are the phase plots with contouring at $z = 5$ m, 7 m, 10 m and 13 m. At $z = 5$ m, the majority of the particles are well bunched. At $z = 7$ m, 12 out of 20 particles are trapped by the ponderomotive potential wells; the same 12 particles remain trapped even at $z = 13$ m. Since the amplitude of the ponderomotive potential is proportional to the radiation field it increases as the radiation field increases. Once the particles are trapped the particles remain trapped and continually lose energy if the pump period, l, is decreased adiabatically.

It should be noted that it is not appropriate to simply increase the pump magnetic field amplitude as a function of axial position in order to enhance efficiency.[37] Increasing B_o spatially deepens the ponderomotive potential well but it also slows down the axial electron velocity and thus synchronism is lost. To maintain synchronism k_o must also be increased.

ACKNOWLEDGMENTS

We have enjoyed stimulating discussions with R. A. Smith, D. L. Granatstein, and I. B. Bernstein.

Appendix A

GENERAL NON-LINEAR FORMULATION

In this appendix, we outline the general formulation of the FEL equations taking into account spatial harmonics in the magnetic pump field as well as spatial and temporal harmonics in the scattered fields. Furthermore, the polarization of the electromagnetic field is arbitrary and permitted to evolve according to the non-linear particle field dynamics.

The vector potential of the periodic pump field containing spatial harmonics of variable amplitudes and wave numbers is expressed as

$$\mathbf{A}_o(z) = \sum_{m=1} A_{o,m}(z) \left\{ \cos\left[m \int_o^z k_o(z')\,dz'\right] \hat{e}_x + \sin\left[m \int_o^z k_o(z')\,dz'\right] \hat{e}_y \right\}, \tag{A1}$$

where the amplitude and fundamental wavenumber are slowly varying function of z. This field is not curl free, but is a good approximation to the exact helically symmetric field near the $r = 0$ axis, when $mk_o r_o < 1$, where r_o is the radius of the electron beam. The pump magnetic field associated with (A1) is given by

$$\mathbf{B}_o(z) = \sum_{m=1} B_{o,m}(z) \left\{ \cos\left[m \int_o^z k_o(z')\,dz' + \varphi_m(z)\right] \hat{e}_x + \sin\left[m \int_o^z k_o(z')\,dz' + \varphi_m(z)\right] \hat{e}_y \right\},$$

where

$$B_{o,m}(z) = -\left[(m\ k_o(z) A_{o,m}(z))^2 + \left[\frac{\partial A_{o,m}(z)}{\partial z}\right]^2\right]^{1/2},$$

and

$$\varphi_m(z) = -\tan^{-1}\left\{\left[\frac{\partial A_{o,m}(z)}{\partial z}\right] \Big/ (m\ k_o(z) A_{o,m}(z))\right\}$$

are slowly varying functions of z. The period of the mth spatial harmonic of the pump magnetic field is a function of z and is

$$l_m(z) = 2\pi \Big/ \left| m\ k_o(z) + \left| \frac{\partial \varphi_m(z)}{\partial z} \right| \right|,$$

where

$$m\ k_o(z) >> \left| \frac{\partial \varphi_m(z)}{\partial z} \right|$$

Similarly the general form for the scattered electromagnetic field and electrostatic field in terms of the vector potential $\mathbf{A}(z,t)$, and scalar potential $\phi(z,t)$

$$\mathbf{A}(z,t) = \sum_{n=1} \left\{ A_{x,n}(z) \cos\left[n \int_o^z k_{x,n}(z')dz' - n\omega t + \theta_{x,n} \right] \hat{e}_x \right.$$
$$\left. + A_{y,n}(z) \sin\left[n \int_o^z k_{y,n}(z')dz' - n\omega t + \theta_{y,n} \right] \hat{e}_y \right\}, \tag{A2}$$

and

$$\phi(z,t) = \sum_{l=1} \phi_l(z) \cos\left[l \int_o^z k_l(z')dz' - l\omega t + \theta_{x,l} \right], \tag{A3}$$

where the amplitudes of the potentials $A_{x,n}(z)$, $A_{y,n}(z)$, and $\phi_l(z)$ as well as wave numbers $k_{x,n}(z)$, $k_{y,n}(z)$ and $k_l(z)$ are slowly varying functions of z.

Using the same procedure as used to derive Eqs. (7a-f) we obtain the following set of equations for the spatially slowly varying amplitudes and wavenumbers.

$$n^2\left[\frac{\omega^2}{c^2} - k_{x,n}^2(z) \right] A_{x,n}(z) = \frac{-4\omega}{c} \int_o^{\frac{2\pi}{\omega}} J_x(z,t) \cos\left[n \int_o^z k_{x,n}(z')dz' - n\omega t + \theta_{x,n} \right] dt_o.$$

$$2n\ k_{x,n}^{1/2}(z) \frac{\partial}{\partial z}\left[A_{x,n}(z) k_{x,n}^{1/2}(z) \right] = \frac{4\omega}{c} \int_o^{\frac{2\pi}{\omega}} J_x(z,t) \sin\left[n \int_o^z k_{x,n}(z')dz' - n\omega t + \theta_{x,n} \right] dt_o.$$

$$n^2\left[\frac{\omega^2}{c^2} - k_{y,n}^2(z) \right] A_{y,n}(z) = \frac{4\omega}{c} \int_o^{\frac{2\pi}{\omega}} J_y(z,t) \sin\left[n \int_o^z k_{y,n}(z')dz' - n\omega t + \theta_{y,n} \right] dt_o.$$

$$2n\ k_{y,n}^{1/2}(z)\ \frac{\partial}{\partial z}\left[\ A_{y,n}(z)\,k_{y,n}^{1/2}(z)\right] = \frac{4\omega}{c}\int_o^{\frac{2\pi}{\omega}} J_y(z,t)\ \cos\left[n\int_o^z k_{y,n}(z')\,dz' - n\omega t + \theta_{y,n}\right]dt_o.$$

$$l\frac{\partial\phi_l(z)}{\partial z} = 4\int_o^{\frac{2\pi}{\omega}} J_z(z,t)\ \sin\left[l\int_o^z k_l(z')\,dz' - l\omega t + \theta_{z,l}\right]dt_o.$$

$$l^2 k_l\,\phi_l(z) = 4\int_o^{\frac{2\pi}{\omega}} J_z(z,t)\ \cos\left[l\int_o^z k_l(z')\,dz' - l\omega t + \theta_{z,l}\right]dt_o. \qquad \text{(A4a-f)}$$

Substituting the expressions for $\mathbf{J}(z,t)$ from Eq. (13), into the Eqs. (A4a-f) and integrating, we obtain

$$n^2\left[\frac{\omega^2}{c^2} - k_{x,n}^2(z)\right] A_{x,n}(z)$$
$$= 4|e|n_o\,\frac{v_{z0}}{c}\omega\int_o^{2\pi/\omega}\frac{\eta_x(t_o,\tau(t_o,z))}{\eta_z(t_o,\tau(t_o,z))}\cos\left[n\int_o^z k_{x,n}(z')\,dz' - n\omega\tau(t_o,z) + \theta_{x,n}\right]dt_o.$$

$$2n\ k_{x,n}^{1/2}(z)\ \frac{\partial}{\partial z}\left[\ A_{x,n}(z)\,k_{x,n}^{1/2}(z)\right]$$
$$= -4|e|n_o\,\frac{v_{z0}}{c}\omega\int_o^{2\pi/\omega}\frac{\eta_x(t_o,\tau(t_o,z))}{\eta_z(t_o,\tau(t_o,z))}\sin\left[n\int_o^z k_{x,n}(z')\,dz' - n\omega\tau(t_o,z) + \theta_{x,n}\right]dt_o.$$

$$n^2\left[\frac{\omega^2}{c^2} - k_{y,n}^2(z)\right] A_{y,n}(z)$$

$$= -4|e|n_o\,\frac{v_{z0}}{c}\omega\int_o^{2\pi/\omega}\frac{\eta_y(t_o,\tau(t_o,z))}{\eta_z(t_o,\tau(t_o,z))}\sin\left[n\int_o^z k_{y,n}(z')\,dz' - n\omega\tau(t_o,z) + \theta_{y,n}\right]dt_o.$$

$$2n\ k_{y,n}^{1/2}(z)\ \frac{\partial}{\partial z}\left[\ A_{y,n}(z)\,k_{y,n}^{1/2}(z)\right]$$
$$= -4|e|n_o\,\frac{v_{z0}}{c}\omega\int_o^{2\pi/\omega}\frac{\eta_y(t_o,\tau(t_o,z))}{\eta_z(t_o,\tau(t_o,z))}\cos\left[n\int_o^z k_{y,n}(z')\,dz' - n\omega\tau(t_o,z) + \theta_{y,n}\right]dt_o.$$

$$l\ \frac{\partial\phi_l(z)}{\partial z} = -4|e|n_o\ v_{z0}\int_o^{2\pi/\omega}\sin\left[l\int_o^z k_l(z')\,dz' - l\omega\tau(t_o,z) + \theta_{z,l}\right]dt_o.$$

$$l^2 k_l\,\phi_l(z) = -4|e|n_o\ v_{z0}\int_o^{2\pi/\omega}\cos\left[l\int^z k_l(z')\,dz' - l\omega\tau(t_o,z) + \theta_{z,l}\right]dt_o. \qquad \text{(A5a-f)}$$

The expression of the particle orbit equation, (14), remains the same. Equations (14), (A5a-f), and along with the definitions of momenta,

$$\eta_x(z,\tau) = \frac{|e|}{c}(A_{o,x}(z) + A_x(z,\tau)),$$
$$\eta_y(z,\tau) = \frac{|e|}{c}(A_{o,y}(z) + A_y(z,\tau)),$$

and

$$\eta_z(z,\tau) = m_o\gamma(z,\tau)V_z(z,\tau), \tag{A6}$$

form the full set of self-consistent FEL equations.

Setting $n = m = l = 1$, and requiring $k_{x,1}(z) = k_{y,1}(z) = k_+(z)$ and $A_{x,1}(z) = A_{y,1}(z) = A(z)$, equations (A5a-f) reduce to the fundamental harmonic equations in (22a,b) and (23a,b) for a circularly polarized electromagnetic field.

REFERENCES

1. H. Motz, J. Appl. Phys. **22**, 527 (1951).

2. J.M.J. Madey, J. Appl. Phys. **42**, 1906 (1971).

3. R.B. Palmer, J. Appl. Phys. **43**, 3014 (1972).

4. V.P. Sukhatme and P.W. Wolff, J. Appl. Phys. **44**, 2331 (1973).

5. J.M.J. Madey, H.A. Schwettman and W.M. Fairbank, IEEE Trans. Nucl. Sci. **20**, 980 (1973).

6. A.T. Lin and J.M. Dawson, Phys. Fluids **18**, 201 (1975).

7. A. Hasegawa, K. Mima, P. Sprangle, H.H. Szu and V.L. Granatstein, Appl. Phys. Lett. **29**, 542 (1976).

8. F.A. Hopf, P. Meystre, M.O. Scully and W.H. Louisell, Phys. Rev. Lett. **37**, 1342 (1976).

9. F.A. Hopf, P. Meystre, M.O. Sully and W.H. Louisell, Optics Comm. **18**, 413 (1976).

10. W B. Colson, Phys. Lett. **59A**, 187 (1976).

11. N.M. Kroll and W.A. McMullin, Phys. Rev. **A17**, 300 (1978).

12. P. Sprangle and V.L. Granatstein, Phys. Rev. **A17**, 1792 (1978).

13. S.B. Segall, Report No. KMSF-U806 Oct. (1978).

14. L.R. Elias, Phys Rev. Lett. **42**, 977 (1979).

15. P. Sprangle and A.T. Drobot, J. Appl. Phys. **50**, 2652 (1979).

16. I.B. Bernstein and J.L. Hirshfield, Phys. Rev. Lett. **40**, 761 (1978).

17. P. Sprangle, R.A. Smith and V.L. Granatstein, NRL Memo. Report 3911 (1978). (To be published in *Infrared and Millimeter Waves*, Vol. I, K. Button (ed.), Academic Press, 1979).

18. P. Sprangle and R.A. Smith, NRL Memo. Report 4033 (1979).

19. P. Sprangle and V.L. Granatstein, Appl. Phys. Lett. **25**, 377 (1974).

20. W.M. Manheimer and E. Ott, Phys. Fluids **17**, 706 (1974).

21. V.I. Miroshnichenko, Sov. Tech. Phys. Lett. **1**, 453, (1975).

22. P. Sprangle, V.L. Granatstein and L. Baker, Phys. Rev. **A12**, 1697 (1975).

23. A. Kwan, J.M. Dawson and A.T. Lin, Phys. Fluid **20**, 581 (1977).

24. W. Colson and S. Ride, private communication.

25. V.L. Granatstein and P. Sprangle, IEEE Trans. MTT-25, 545 (1977).

26. A. Hasegawa, Bell System Tech. J. **57**, 3069 (1978).

27. C.W. Planner, Phys. Lett. **67A**, 263 (1978).

28. L.R. Elias, W.M. Fairbank, J.M.J. Madey, H.A. Schwettman and T.I. Smith, Phys. Rev. Lett. **36**, 717 (1976).

29. D.A.G. Deacon, L.R. Elias, J.M.J. Madey, G.J. Ramian, H.A. Schwettman and T.I. Smith, Phys. Rev. Lett. 38, 892 (1977).

30. V.L. Granatstein, M. Herndon, R.K. Parker and S.P. Schlesinger, IEEE Trans. Microwaves Theory Tech. MITT-22, 1000 (1974).

31. J. Nation, J. Appl. Phys., to be published (1979).

32. V.L. Granatstein, S.P. Schlesinger, M. Herndon, R.K. Parker and J.A. Pasour, Appl. Phys. Lett. 30, 384 (1977).

33. D.B. McDermott, T.C. Marshall, S.P. Schlesinger, R.K. Parker and V.L. Granatstein, Phys. Rev. Lett. 41, 1368 (1978).

34. R.M. Gilgenbach, T.C. Marshall and S.P. Schlesinger, Phys. Fluids, 22, 971 (1978).

35. T.C. Marshall, S. Talmadge, and P. Efthimion, App. Phys. Lett. 31, 320-322 (1977).

36. To our knowledge this technique for enhancing efficiency is also being analyzed by N.M. Kroll and coworkers (private communications).

37. While this work was being submitted, the paper by A.T. Lin and J.M. Dawson, Phys. Rev. Lett 42, 1670 (1979), dealing with efficiency enhancement by increasing the magnetic pump amplitude, came to the authors' attention.

Table I — Optical and Submillimeter Illustrations of FELs
(Constant Magnetic Pump Parameters)

Magnetic Pump Parameters		Example #1	Example #2
Pump Wavelength	l	1.5 cm	2.0 cm
Pump Amplitude	B_o	6.0 kG	2.5 kG
Electron Beam Parameters			
Beam Energy	E_o	66 MeV ($\gamma_o = 131$)	2.6 MeV($\gamma_o = 6$)
Beam Current	I_o	2 kA	5 kA
Axial Gamma	γ_{zo}	100	5.4
Beam Radius	r_o	0.1 cm	0.3 cm
Equil. ⊥ Velocity	$\beta_{o\perp}$	6.4×10^{-3}	0.078
Critical ⊥ Velocity	β_{crit}	1.5×10^{-3}	0.22
Beam Strength Parameter	ξ	0.14	0.87
Self Potential Energy Spread	$\Delta E/E_o$	0.08%	1.7%
Output Radiation Parameters			
Radiation Wavelength	λ	0.75 μm	338 μm
Linear e-folding length*	$L_e = -\mathrm{Im}(k)^{-1}$	38 cm	5.3 cm
Efficiency*	η	0.52%	9.2%
Saturated A-Field*	A	33 volts	7.4×10^3 volts
Radiation Power*	P_o	0.69 GW	1.2 GW

*For maximum growth rate.

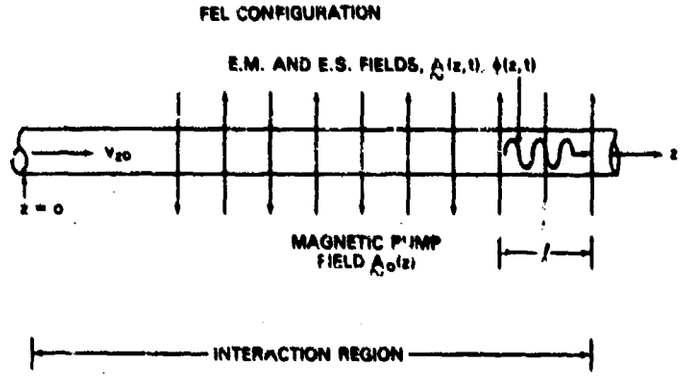

Fig. 1 — Schematic of the free-electron laser model. The unmodulated electron beam enters the interaction region from the left. The pump field builds up adiabatically and reaches a constant amplitude for $z > 0$.

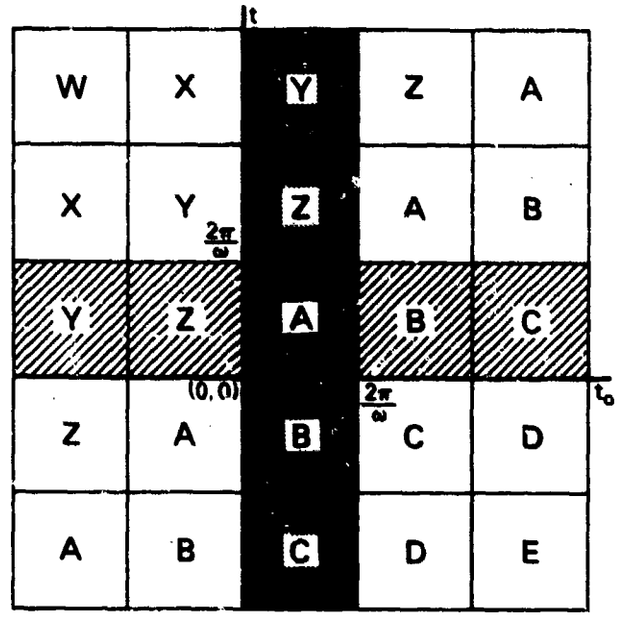

Fig. 2 — A diagram to illustrate the symmetry property of the function $G(t_0, z, t)$ in the (t, t_0) plane.

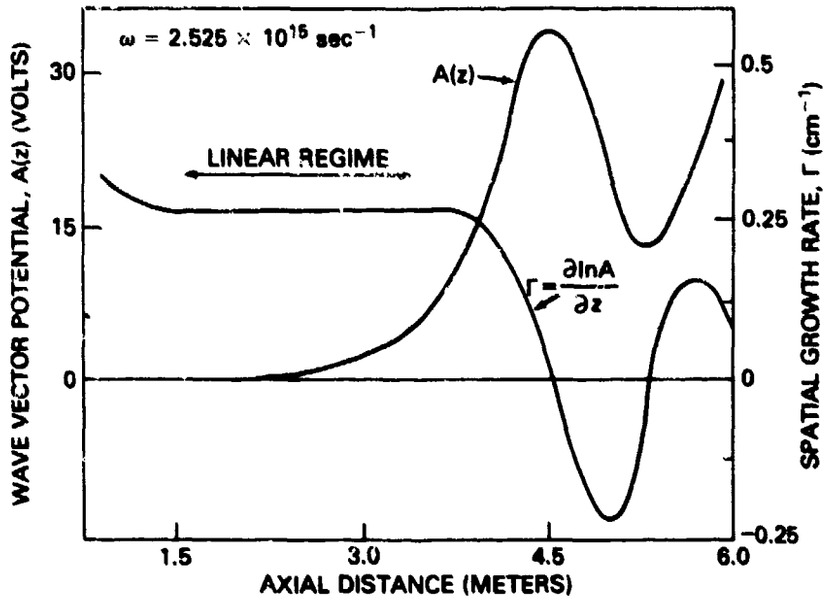

Fig. 3 — Wave vector potential $A(z)$ and spatial linear growth rate Γ as a function of axial distance for example 1 in the optical regime. The frequency is chosen to give the maximum linear spatial growth rate.

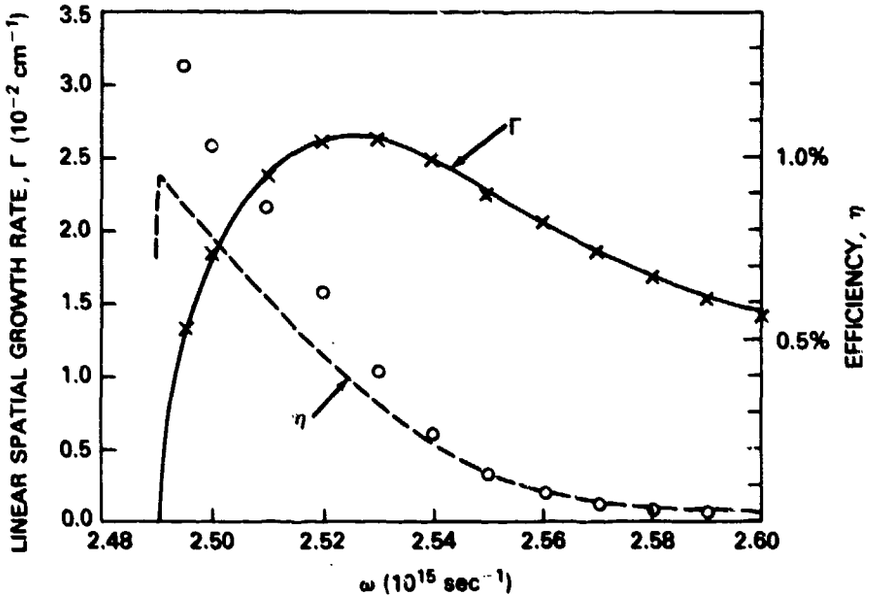

Fig. 4 — A comparison of the growth rate in the linear regime of the non-linear simulation (crosses (x)) with the growth rate from linear theory (solid curve), and a comparison of efficiency from non-linear theory (circles (O)) with that from linear theory using trapping arguments (dashed curve) as a function of frequency for example 1.

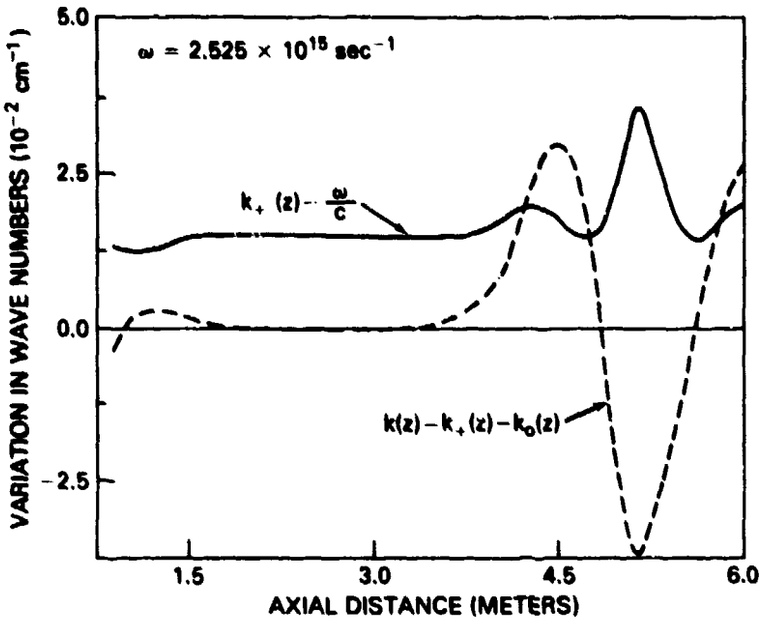

Fig. 5 — The variation in wavenumber of the scattered radiation $k_+(z)$ and the variation in wavenumber of the space charge potential $k(z)$ as a function of axial distance for example 1 at the frequency corresponding to maximum linear spatial growth.

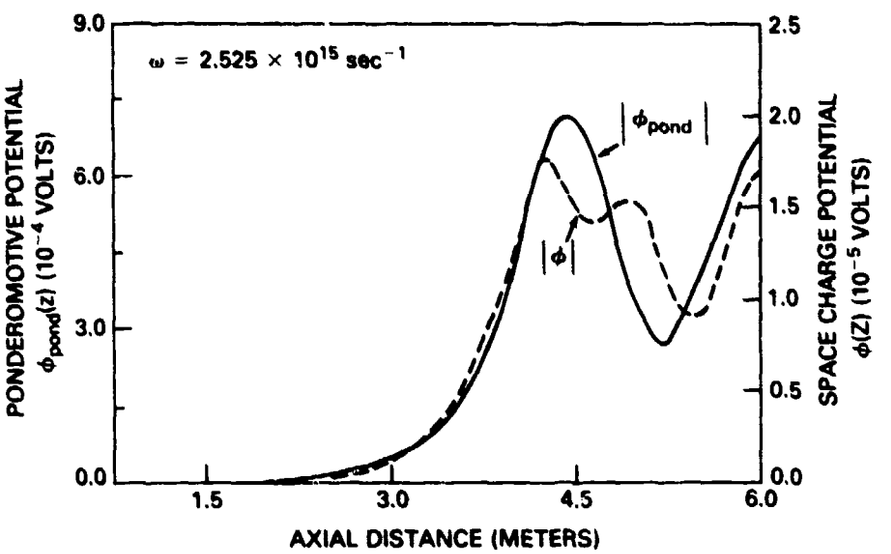

Fig. 6 — A comparison of the magnitude of the ponderomotive potential $|\phi_{pond}(z)|$ and the space charge potential $|\phi(z)|$ as a function of axial distance for example 1 at the frequency corresponding to maximum linear spatial growth.

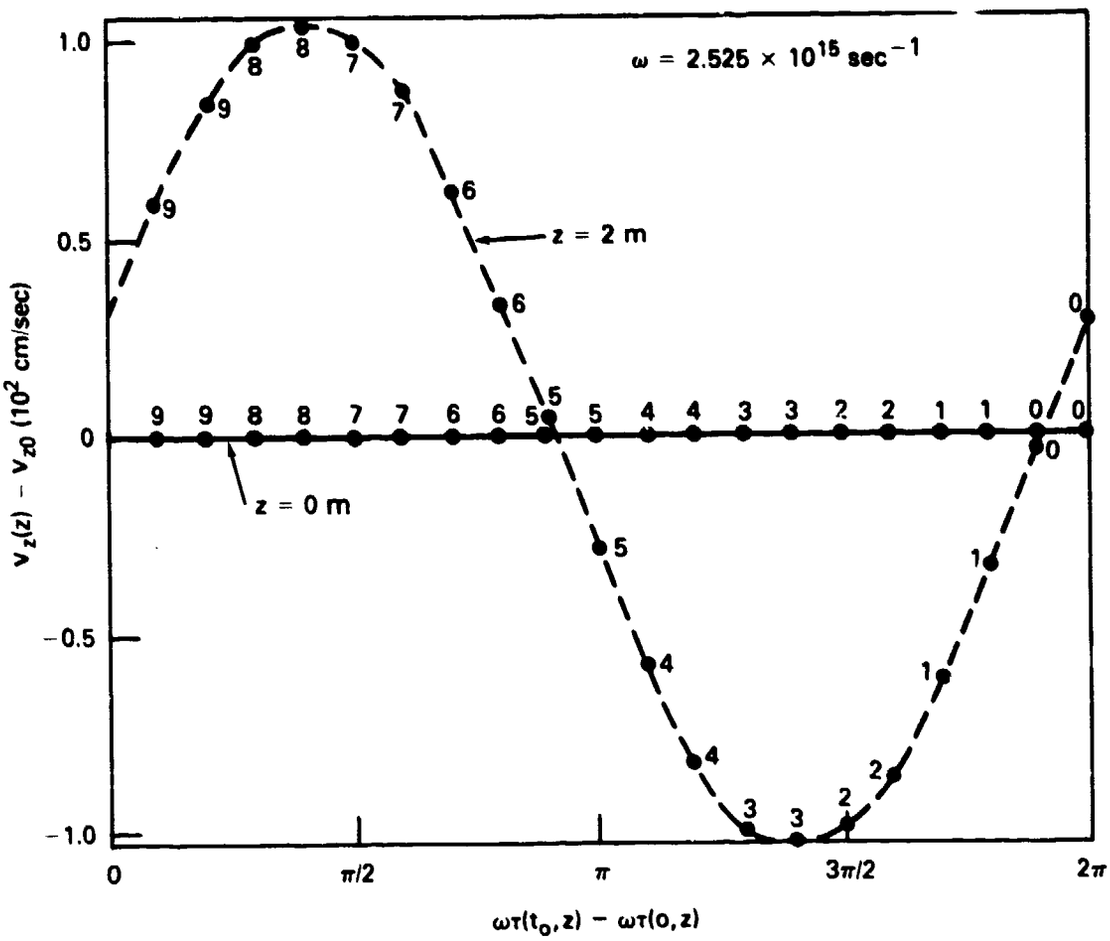

(a)

Fig. 7 — Phase space plots of velocity versus the relative time the particles in one beamlet cross the following axial positions (a) z = 0.0 m and z = 2.0 m, (b) z = 4.0 m, (c) z = 4.3 m and (d) z = 45 m for example 1

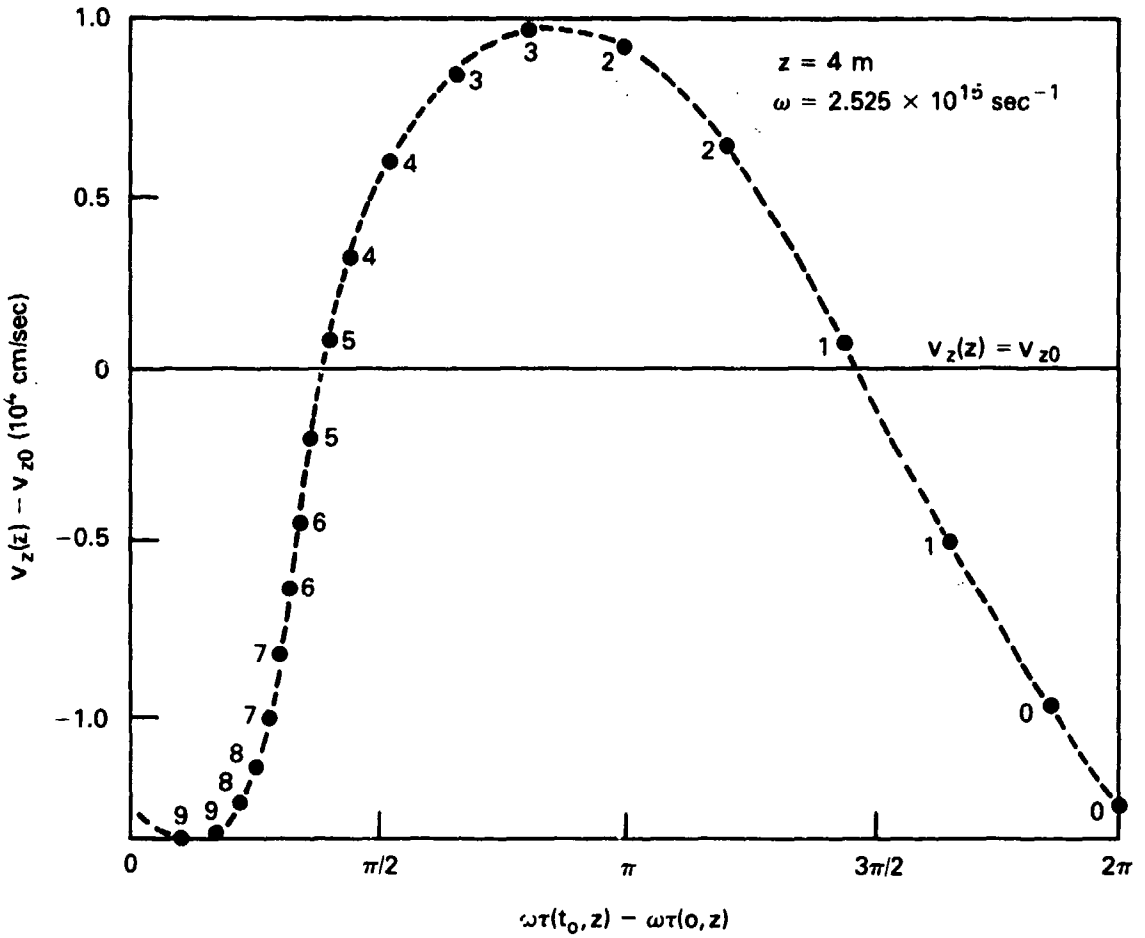

(b)

ig. 7 (Continued) — Phase space plots of velocity versus the relative time the particles in one beamlet cross the following axial positions (a) $z = 0.0$ m and $z = 2.0$ m, (b) $z = 4.0$ m, (c) $z = 4.3$ m and (d) $z = 45$ m for example 1

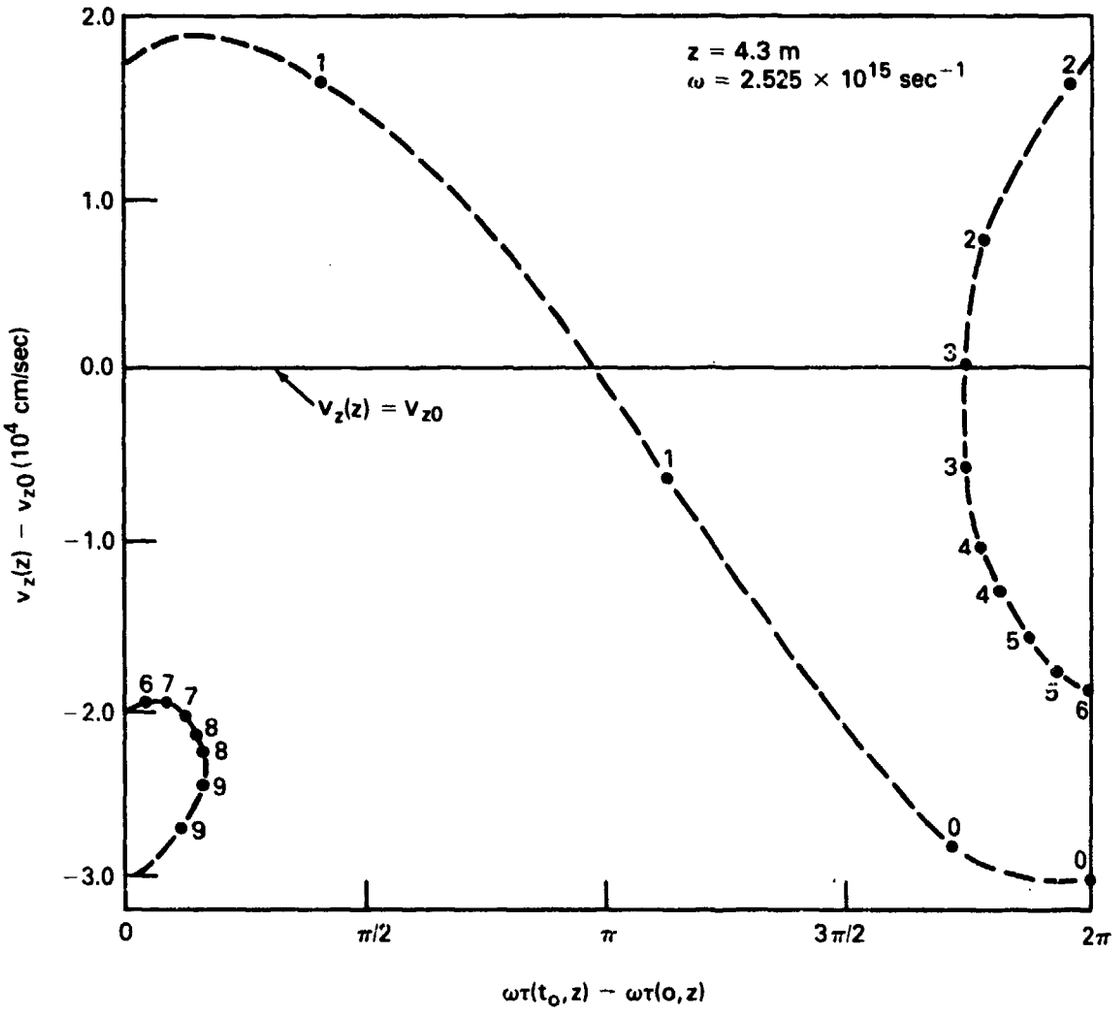

(c)

Fig. 7 (Continued) — Phase space plots of velocity versus the relative time the particles in one beamlet cross the following axial positions (a) $z = 0.0$ m and $z = 2.0$ m, (b) $z = 4.0$ m, (c) $z = 4.3$ m and (d) $z = 45$ m for example 1

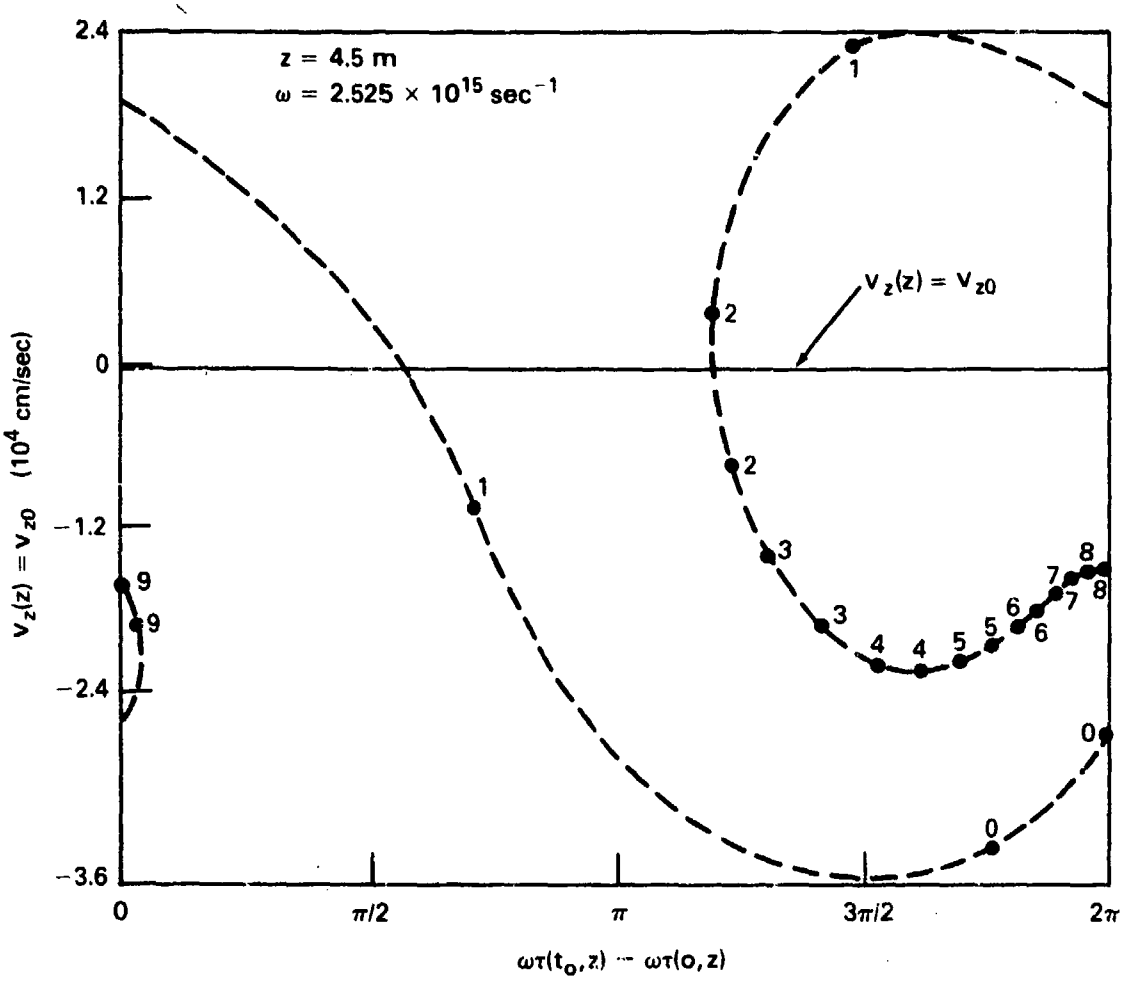

(d)

Fig. 7 (Continued) — Phase space plots of velocity versus the relative time the particles in one beamlet cross the following axial positions (a) $z = 0.0$ m and $z = 2.0$ m, (b) $z = 4.0$ m, (c) $z = 4.3$ m and (d) $z = 45$ m for example 1

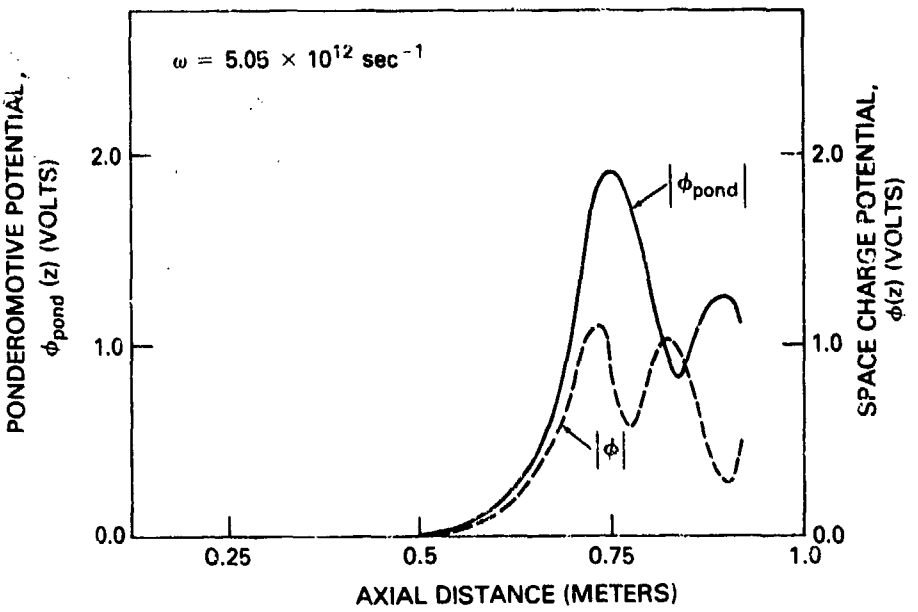

Fig. 8 — A comparison of the magnitude of the ponderomotive potential $|\phi_{pond}(z)|$ and the space charge potential $|\phi(z)|$ as a function of axial distance for example 2 at the frequency corresponding to maximum linear spatial growth.

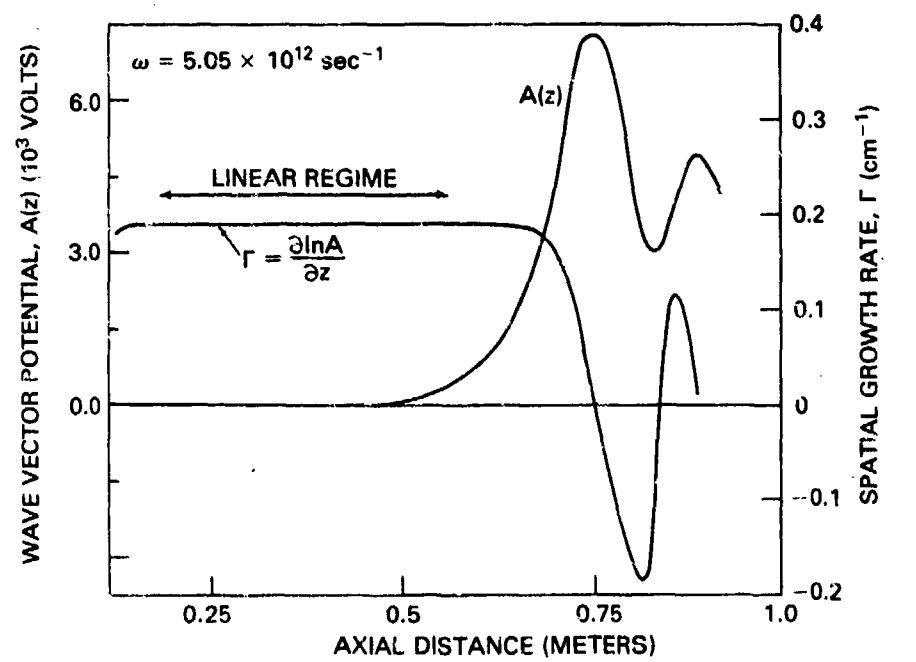

Fig. 9 — The wave vector potential $A(z)$ and the spatial growth rate Γ as a function of axial distance for example 2 at the frequency corresponding to maximum linear growth.

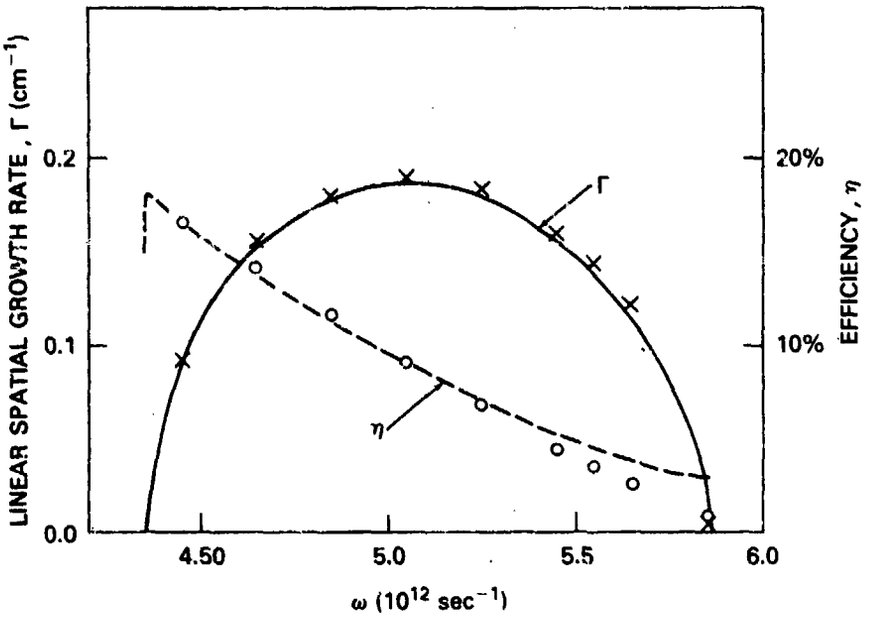

Fig. 10 — A comparison of the growth rate in the linear regime of the non-linear simulation (crosses (x)) with the growth rate from linear theory (solid curve), and a comparison of efficiency from the non-linear theory (circles (O)) with that from linear theory using trapping arguments (dashed curve) as a function of frequency for example 2.

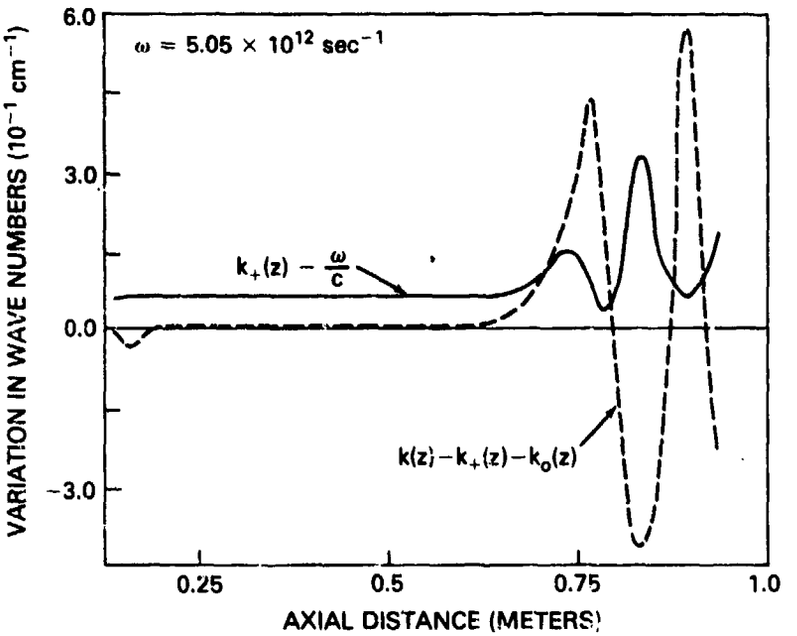

Fig. 11 — The variation in wavenumber of the scattered radiation $k_+(z)$ and the variation in wavenumber of the space charge potential $k_0(z)$ as a function of axial distance for example 2 at the frequency corresponding to maximum linear spatial growth.

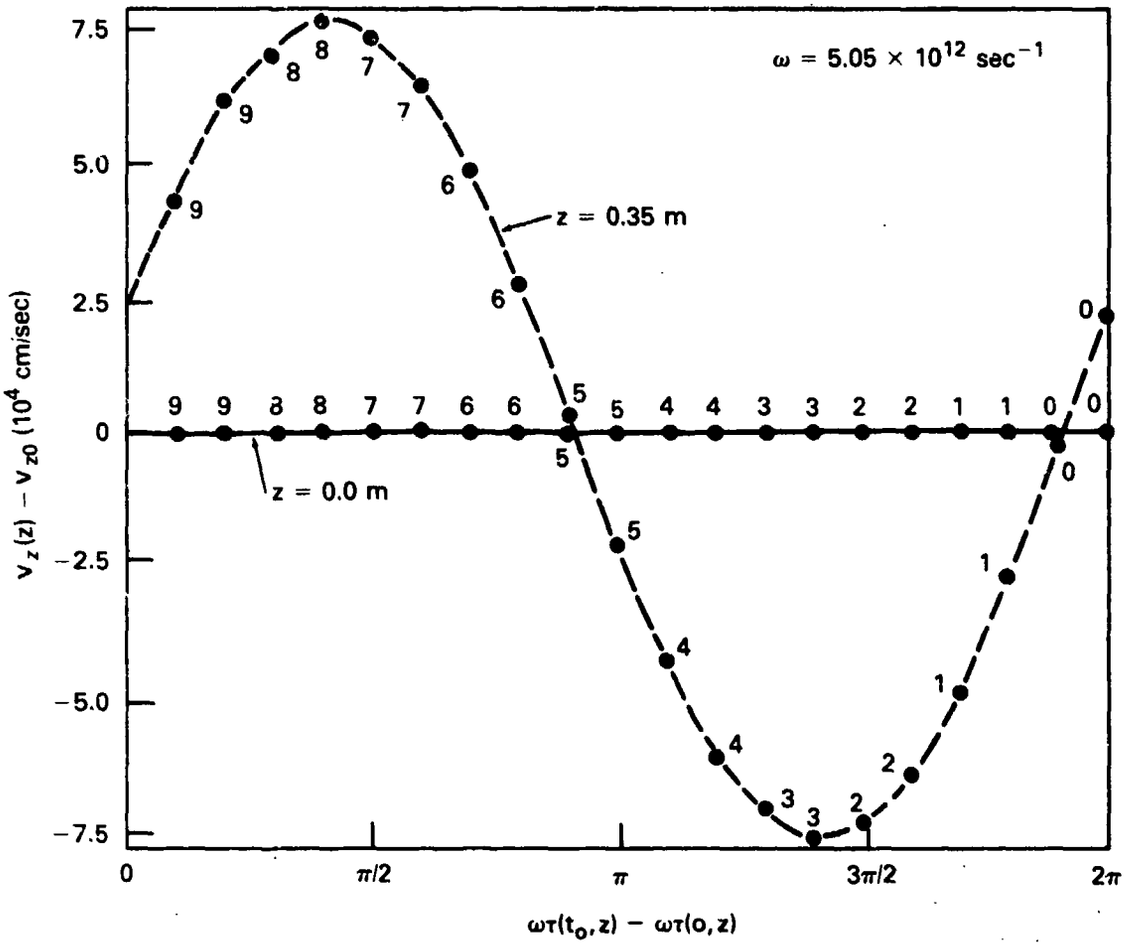

(a)

Fig. 12 — Phase space plots of velocity versus the relative time the particles in one beamlet cross the following axial positions (a) $z = 0.0$ m and $z = 0.35$ m, (b) $z = 0.7$ m and (c) $z = 0.77$ m for example 2

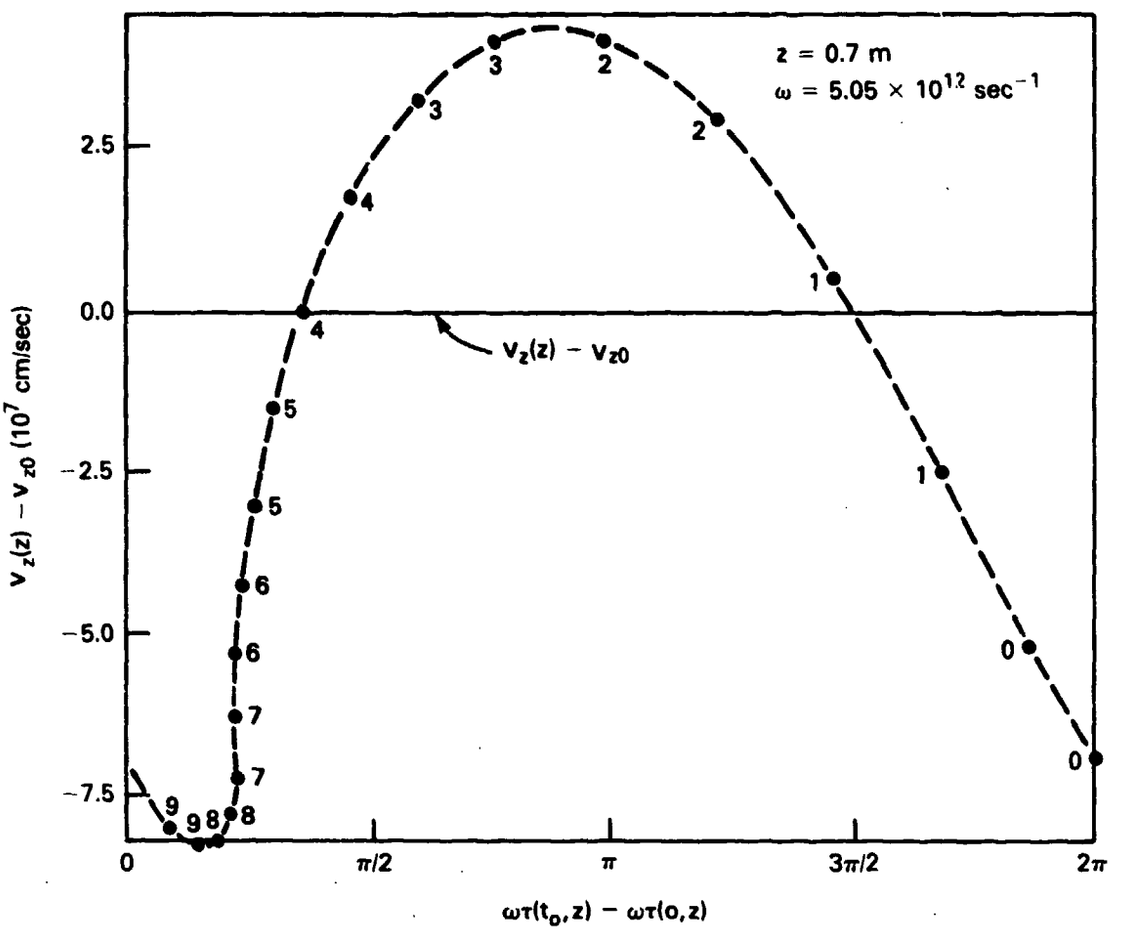

(b)

Fig. 12 (Continued) — Phase space plots of velocity versus the relative time the particles in one beamlet cross the following axial positions (a) $z = 0.0$ m and $z = 0.35$ m, (b) $z = 0.7$ m and (c) $z = 0.77$ m for example 2

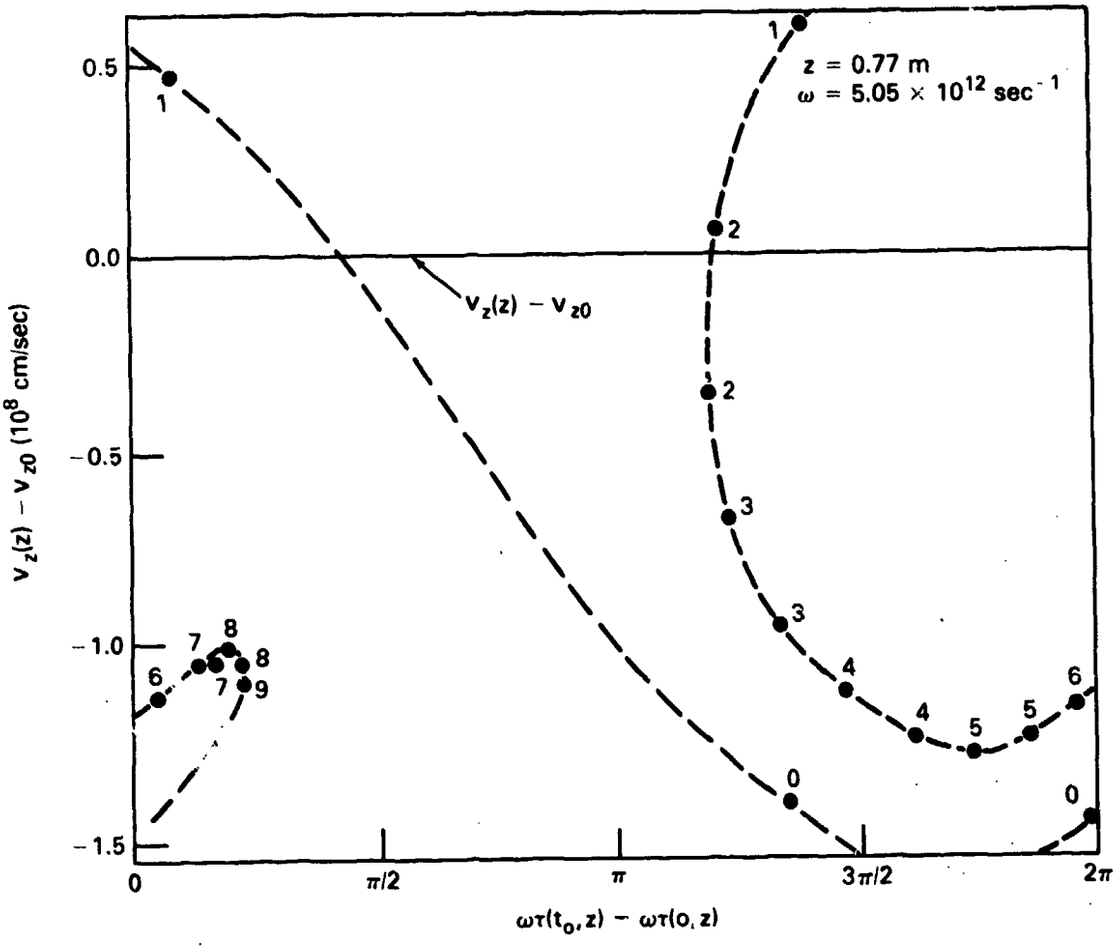

(c)

Fig. 12 (Continued) — Phase space plots of velocity versus the relative time the particles in one beamlet cross the following axial positions (a) 0 m and z = 0.35 m, (b) z = 0.7 m and (c) z = 0.77 m for example 2

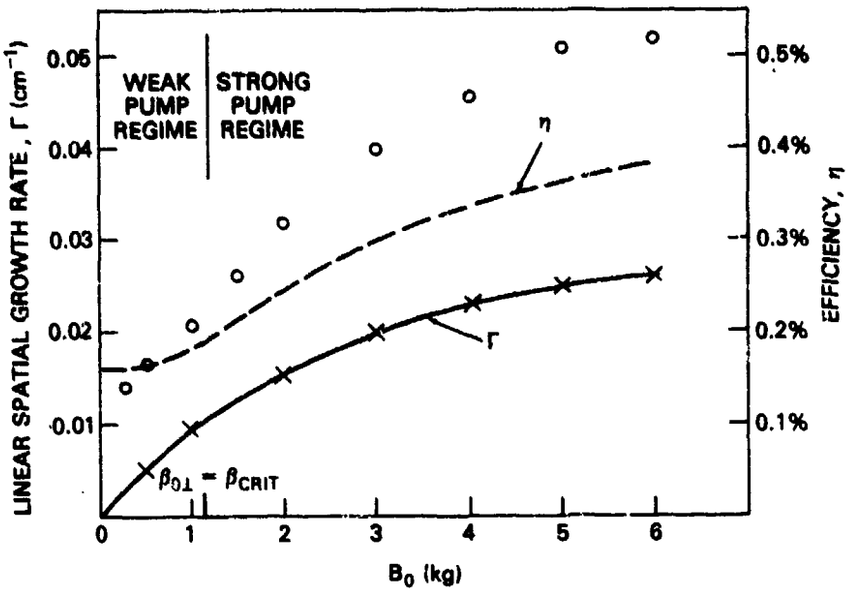

Fig. 13 — A comparison of the maximum growth rate in the linear regime of the non-linear simulation (crosses (x)) with the maximum growth rate from linear theory (solid curve), and a comparison of efficiency from non-linear theory (circles (O)) with that from linear theory using the trapping arguments (dashed curve) as a function of the magnetic pump field amplitude for a fixed output frequency.

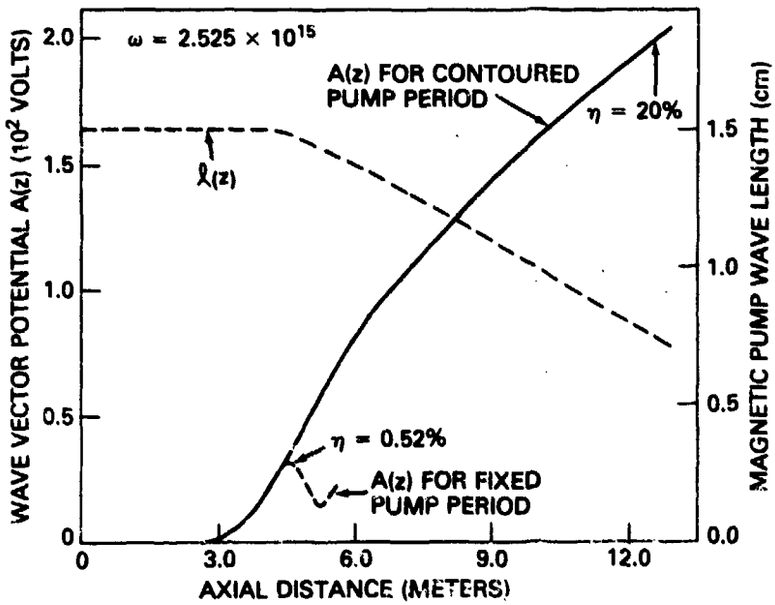

Fig. 14 — Enhancement of radiation field by decreasing the magnetic pump period. The efficiency has increased from 0.52% at $z = 4.5$ m with a constant pump period to 20% at $z = 13$ m with the period of the pump changing as shown.

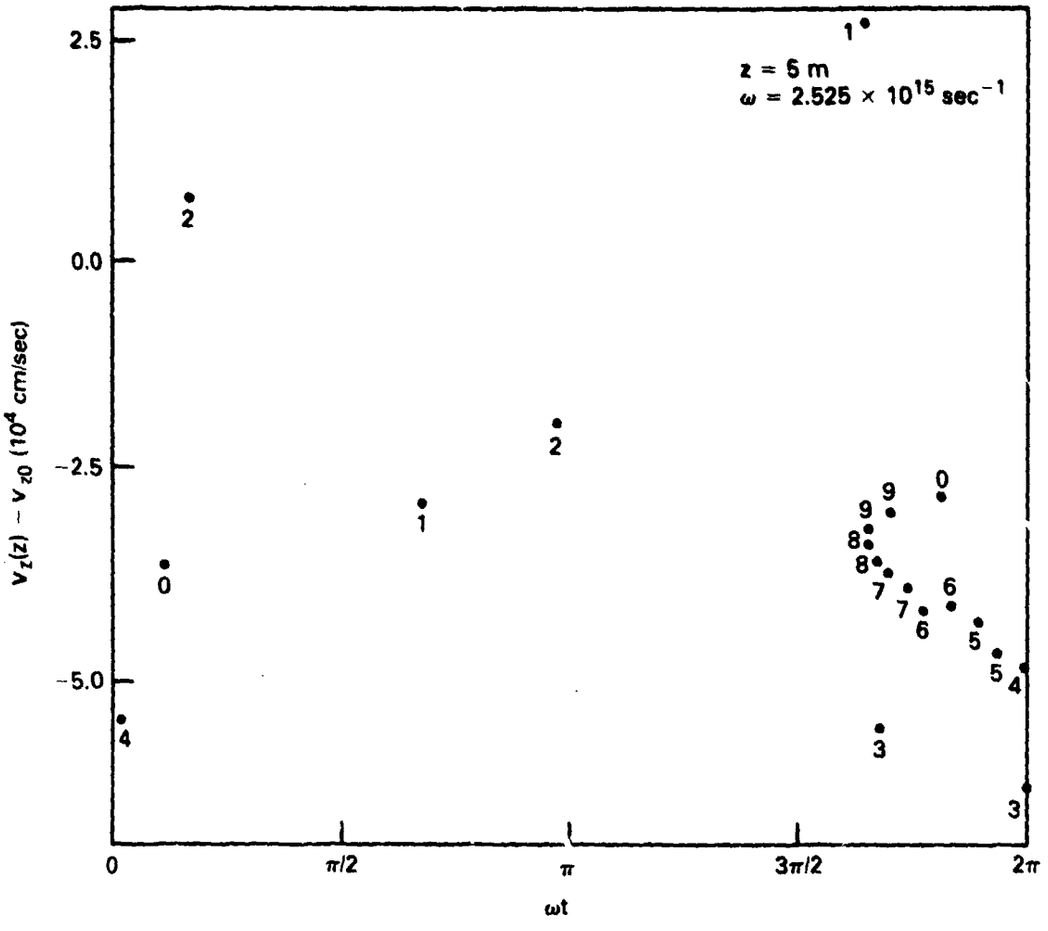

(a)

Fig. 15 — Phase plots with contoured magnetic pump period shown in Fig. (14) at (a) $z = 5$ m, (b) $z = 7$ m, (c) $z = 10$ m and (d) $z = 13$ m

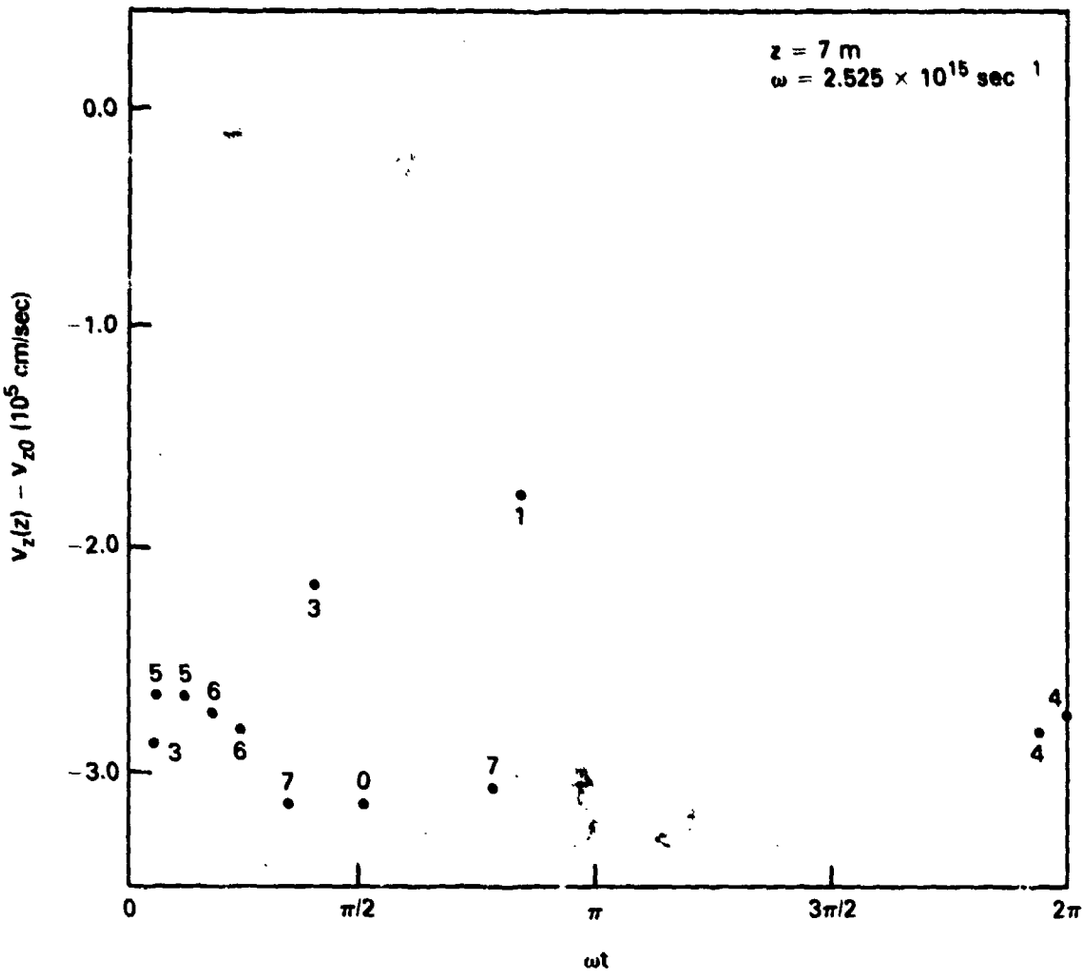

(b)

Fig. 15 (Continued) — Phase plots with contoured magnetic pump period shown in Fig. (14) at (a) $z = 5$ m, (b) $z = 7$ m, (c) $z = 10$ m and (d) $z = 15$ m

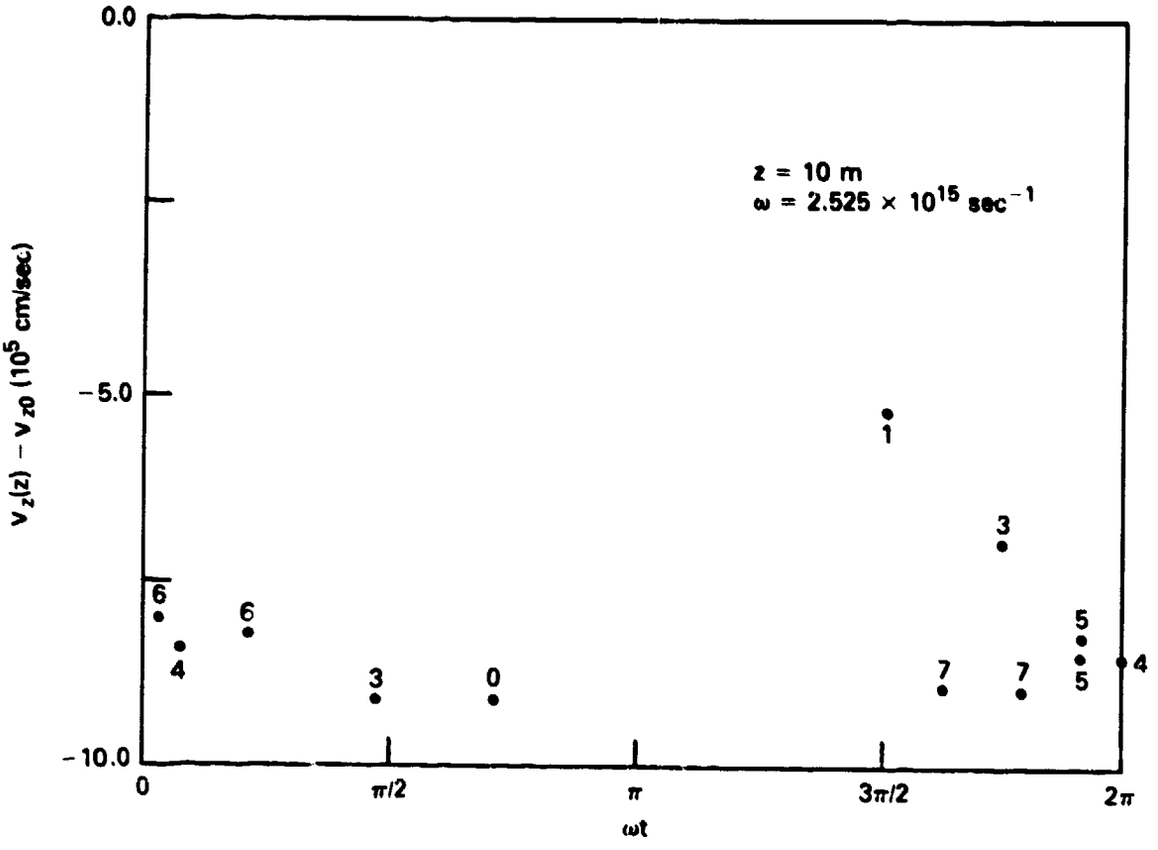

(c)

Fig. 15 (Continued) — Phase plots with contoured magnetic pump period shown in Fig. (14) at (a) $z = 5$ m, (b) $z = 7$ m, (c) $z = 10$ m and (d) $z = 13$ m

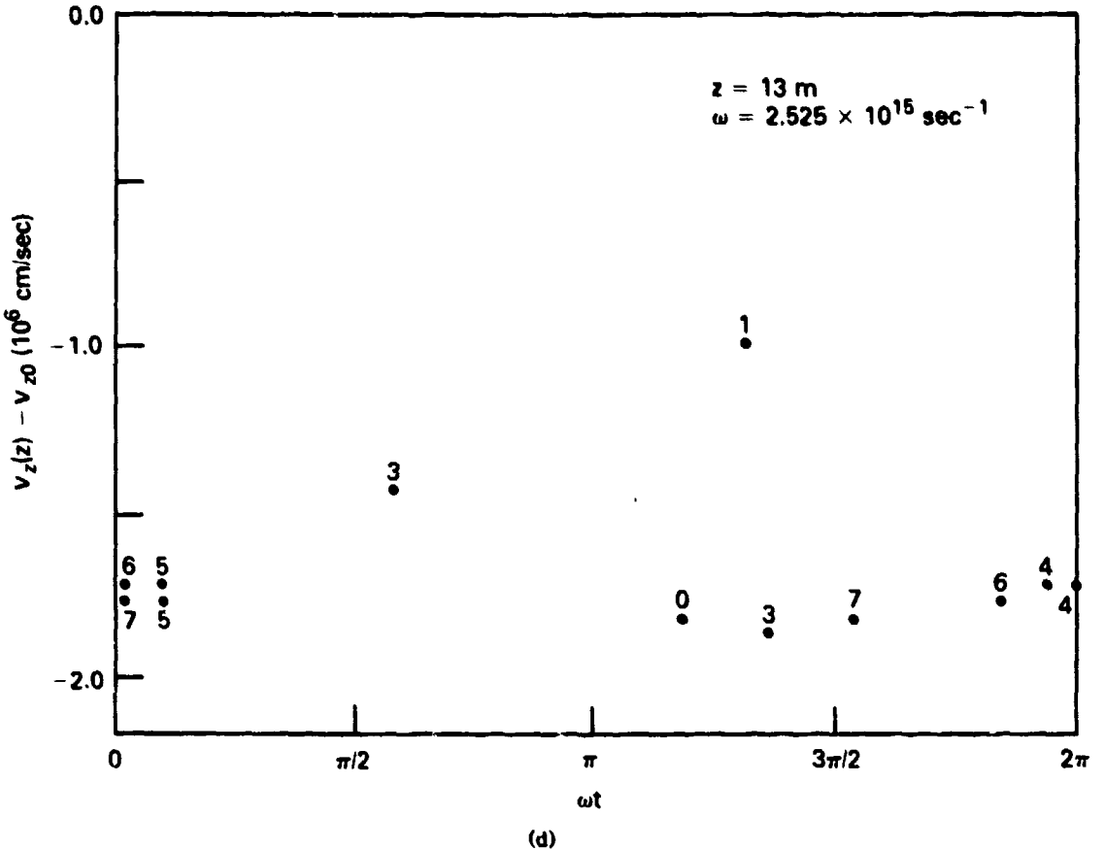

(d)

Fig. 15 (Continued) — Phase plots with contoured magnetic pump period shown in Fig. (14) at (a) $z = 5$ m, (b) $z = 7$ m, (c) $z = 10$ m and (d) $z = 13$ m